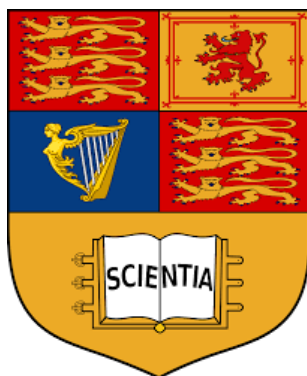


# **Understanding of Charge Carrier Dynamics in Reticular Photocatalytic Materials by Transient Absorption Spectroscopy**



Molecular Science Research Hub, Imperial College London, W12 0BZ

**This report is submitted in partial fulfillment of the requirements for  
the degree of MRes in Nanomaterials, Department of Chemistry**

Author: Shilin Yao

CID: 02062574

Supervisors: Prof James R. Durrant, Dr. Soranyel Gonzalez-Carrero

Submission date: 24th August, 2022

## Abstract

Solar energy utilisation is one of the ideal approaches to mitigate energy crisis. Reticular photocatalysts, such as metal-organic frameworks and covalent organic frameworks, have attracted worldwide attention, due to their ordered and tuneable structure, high modifiability, high specific surface area, and large amount of active sites. However, after years of research, enhancing the efficiency of solar energy conversion and understanding the photocatalytic mechanism are still the most challenging parts. Therefore, we aim to understand the differences in photoactivity of reticular materials by using transient and operando absorption spectroscopies on time scale from picosecond to second, to explain and identify the behaviours of photoactive species generated during photocatalytic process.

In this project, we try to understand why the selected pure metal-organic frameworks are not efficient in photocatalytic CO<sub>2</sub> conversion, by analysing the kinetics of the transient species generated after light irradiation. The transient absorption kinetics revealed fast charge decay, in timescales not optimal for catalysis. We drew a conclusion that an effective strategy is needed for better charge separation. Therefore, we analysed the charge carrier dynamics of covalent organic frameworks with a donor-acceptor structure, and compared it with the dynamics of single component donor and acceptor. It turned out that there are more and longer-lived charges in the heterojunction structure, which proves the effectiveness of heterojunction strategy from photophysical side. This study gives a deeper insight in understanding charge carrier dynamics in reticular photocatalysts and provides guidelines for further improvement on metal-organic framework photocatalysts.

**Keywords:** Transient Absorption Spectroscopy; Photophysics; Covalent Organic Frameworks Heterojunction; Metal-organic Frameworks.

# Table of Contents

ABSTRACT.....	- 1 -
TABLE OF CONTENTS .....	- 2 -
CHAPTER 1 INTRODUCTION.....	- 4 -
CHAPTER 2 AIMS AND OBJECTIVES .....	- 12 -
CHAPTER 3 METHOD .....	- 13 -
3.1 MATERIALS AND CHEMICALS .....	- 13 -
3.2 SAMPLE PREPARATION .....	- 13 -
3.1 MOFs Samples.....	- 13 -
3.2 COFs Samples.....	- 13 -
3.3 PHOTOPHYSICAL STUDY.....	- 14 -
3.3.1 UV-Vis Absorption.....	- 14 -
3.3.2 Photoluminescence (PL) Measurement.....	- 14 -
<i>Both MOFs and COFs samples were measured in solution (acetonitrile as solution for MOFs samples and DMF + Water as solution for COFs) by Cary Eclipse Fluorescence Spectrophotometer.....</i>	- 14 -
3.3.3 Transient Absorption Measurement.....	- 14 -
3.3.4 Photoinduced Absorption Measurement.....	- 15 -
CHAPTER 4 RESULTS AND DISCUSSION.....	- 16 -
4.1 PHOTOPHYSICAL STUDY OF MOFs.....	- 16 -
4.1.1 MOFs Materials.....	- 16 -
4.1.2 UV-Vis Absorption and Photoluminescence Study of MOFs Samples.....	- 16 -
4.1.3 Charge Carrier Dynamics Study of MOFs by Ultrafast Transient Absorption Spectroscopy.....	- 20 -
4.2 PHOTOPHYSICAL STUDY OF COF HETEROJUNCTION .....	- 23 -
4.2.1 The Built of Donor-Acceptor COF Heterojunction.....	- 23 -
4.2.2 UV-Vis Absorption and Photoluminescence Study of COFs Samples.....	- 24 -
4.2.3 Charge Carrier Dynamics Study of COF Heterojunction.....	- 25 -
4.2.3.1 From Femtosecond to Microsecond Timescale .....	- 25 -

---

4.2.3.2 From Microsecond to Millisecond Timescale (by Slow TAS).....	- 29 -
4.2.4 Charge Carrier Dynamics Study of COF Heterojunction with Co-catalyst and/or Scavenger.....	- 31 -
4.2.5 Charge Carrier Dynamics Study of COFs by Photoinduced Absorption Spectroscopy.....	- 35 -
4.2.6 Photocatalytic Activity.....	- 36 -
4.3 COMPARISON TO A BROADER RANGE OF PHOTOCATALYSTS .....	- 37 -
<b>CHAPTER 5 CONCLUSIONS AND FUTURE WORK .....</b>	<b>- 39 -</b>
5.1 CONCLUSIONS .....	- 39 -
5.2 FUTURE WORK.....	- 40 -
<b>ACKNOWLEDGEMENTS.....</b>	<b>- 41 -</b>
<b>ACRONYMS.....</b>	<b>- 41 -</b>
<b>REFERENCES.....</b>	<b>42</b>

## Chapter 1 Introduction

Utilising solar energy is always considered as a promising strategy for alleviating the energy crisis and environmental problems that human beings are facing nowadays, and effective conversion methods are urgent to be developed. Over the past few decades, scientists have developed series of reticular photocatalytic materials which have shown great potential in solar energy conversion application, such as Metal-organic Frameworks (MOFs) and Covalent Organic Frameworks (COFs), due to their high surface area, porous structure and advanced structural flexibility, ect<sup>1</sup>.

For instance, in photocatalytic CO<sub>2</sub> reduction to methanol, MOFs can be exploited due to their high affinity to CO<sub>2</sub>, fast CO<sub>2</sub> uptake dynamics, and their ability to host light harvesters and Cu-based co-catalysts. Besides, the porous structure of MOFs and diffusion kinetics could increase the concentration of CO<sub>2</sub> at the contact of the catalytic active sites. The high porosity of MOFs can boost the efficiency of methanol transport. And the hydrophobicity of MOFs pores is adjustable by tuning the pendant groups of organic linkers, to avoid the competition of photocatalytic water splitting.<sup>2</sup>

One of the current technology-specific challenges of photocatalysis by organic semiconductors is improving charge separation. Currently, most of studies are focusing on inorganic photocatalysts, and only limited amount of studies are for reticular photocatalysts<sup>3,4</sup>. There are reported advances on porphyrin and single atom featured reticular photocatalysts, and material improvement strategies for CO<sub>2</sub> reduction, but very limited photophysical studies on understanding these reticular materials and the photocatalytic process happening in them<sup>5,6</sup>. Therefore, the aim of this research project is to understand the carrier dynamics and charge transfer processes in reticular photocatalytic materials, by identifying the photogenerated transient species and analysing their temporal evolution using transient absorption spectroscopies (TAS) and photoinduced absorption spectroscopy (PIAS), which could be of great help to understand their photocatalytic performance, and thus provide guidance for the design of reticular photocatalysts and photocatalytic systems.

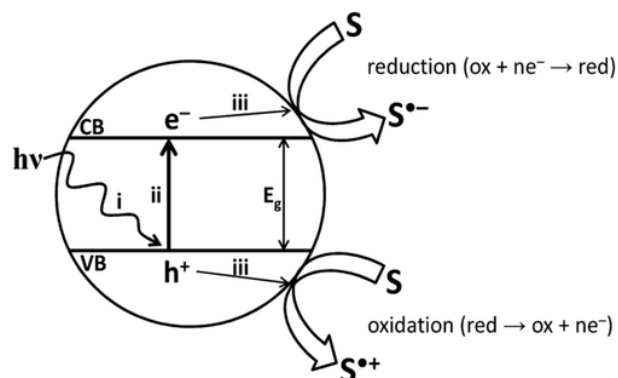


Figure 1 Photocatalytic process in semiconductor photocatalysts<sup>7</sup>

In photocatalytic process, as shown in Figure 1, when the energy of an incident light is higher than the bandgap energy of semiconductor photocatalysts, electrons will be excited to the conduction band and holes will be left on the valence band, and then photocatalytic reactions happen. The traditional inorganic semiconductors are proved not very efficient in photogenerated carrier separation, such as pure  $\text{WO}_3$  and  $\text{CdS}$ <sup>7-9</sup>, but inorganic semiconductors composite with MOFs shows much better behaviour in charge separation<sup>10</sup>. In photocatalysis, generating sufficient long-lived charge carriers is the key factor for the catalytic efficiency. These charge carriers should be spatially separated and live up to milliseconds or seconds to be helpful for photocatalysis, as shown in Figure 2<sup>11</sup>.

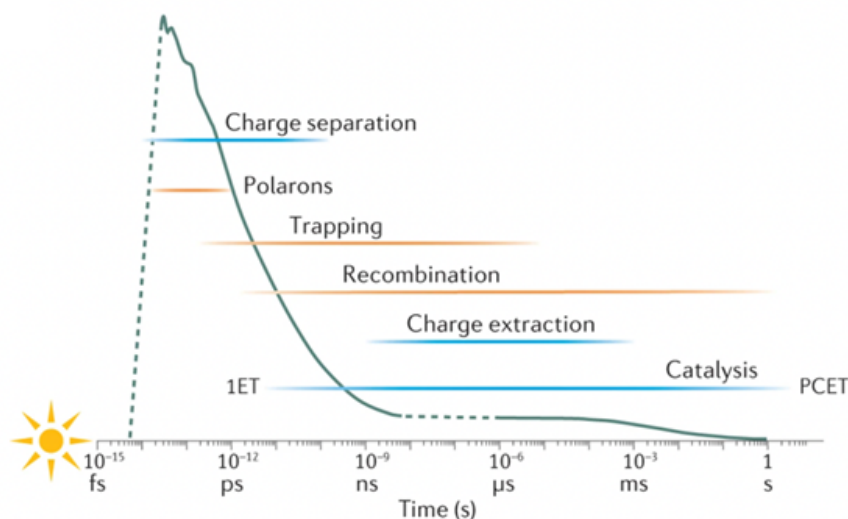


Figure 2 Timescale of charge carrier dynamics from charge generation to catalysis<sup>11</sup>

Compared with traditional inorganic materials (such as  $\text{TiO}_2$  and  $\text{CdS}$ ), reticular organic materials like Metal-organic Frameworks (MOFs) and Covalent Organic Frameworks (COFs), as shown in Figure 3, have increasingly attracted researchers' attention due to their high surface area, high porosity tunability

and great modifiability. Based on reticular design principles, a high level of control in their functionality and accurate prediction of their properties can be achieved<sup>12</sup>.

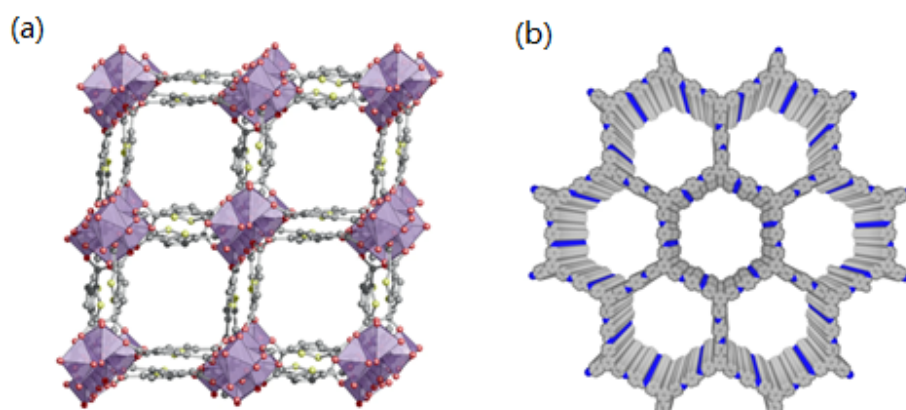


Figure 3 Reticular structure of (a) CAU-23-MOF<sup>13</sup> and (b) TPB-DMeTP-COF<sup>14</sup>

However, in pure MOFs, there are many limitations: such as low electronic conductivity, narrow light absorption range, low stability, and rapid recombination of charges, which greatly impede their industrial applications<sup>15</sup>. To optimise the photocatalytic properties of MOFs, many strategies are developed. For example, in Figure 4 (a), metal ions (non-noble ions such as  $\text{Fe}^{3+}$ ,  $\text{Zn}^{2+}$  and  $\text{Cu}^{2+}$ ; noble ions such as Pt, Ir and Ru) are doped into MOFs units as electron traps to improve charge separation and provide more active sites<sup>15</sup>. The composite of MOFs with metal oxides [such as  $\text{TiO}_2/\text{ZIF-8}$ <sup>16</sup>, Figure 4 (b)], metal sulfides (such as  $\text{CdS}/\text{UiO-66}$ <sup>17</sup>), metal phosphides (such as  $\text{Ni}_2\text{P}/\text{UiO-66-NH}_2$ <sup>18</sup>) or carbon materials (such as  $\text{g-C}_3\text{N}_4$ , carbon dots and carbon nanotubes) are also prepared to improve the charge transfer process in photocatalysis.

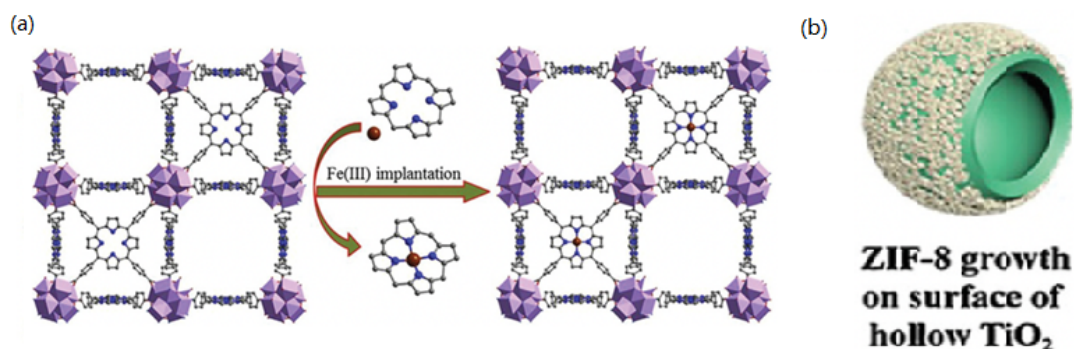


Figure 4 (a)  $\text{Fe}^{3+}$  ion-doped MOF<sup>15</sup> (b)  $\text{TiO}_2/\text{ZIF-8}$ <sup>16</sup>

The photocatalytic mechanism becomes harder to study because of the complexity of material



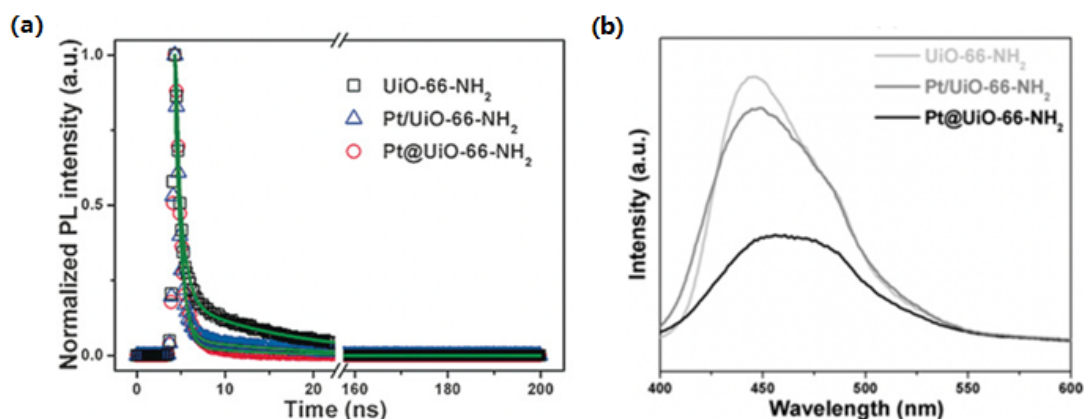


Figure 6 The kinetics(a) and PL(b) comparison of UiO-66-NH<sub>2</sub>, Pt/UiO-66-NH<sub>2</sub> and Pt@UiO-66-NH<sub>2</sub><sup>21</sup>

It is commonly accepted that the photoexcitation process in MIL-125(Ti) is through ligand to metal transfer (LMCT)<sup>22</sup>, and the electron transfer from the linker to the metal ion to reduce it, as shown in Figure 7<sup>23</sup>, same for UiO-66-NH<sub>2</sub> (electron transfer from the ligand to the Zr-O cluster)<sup>24</sup>.

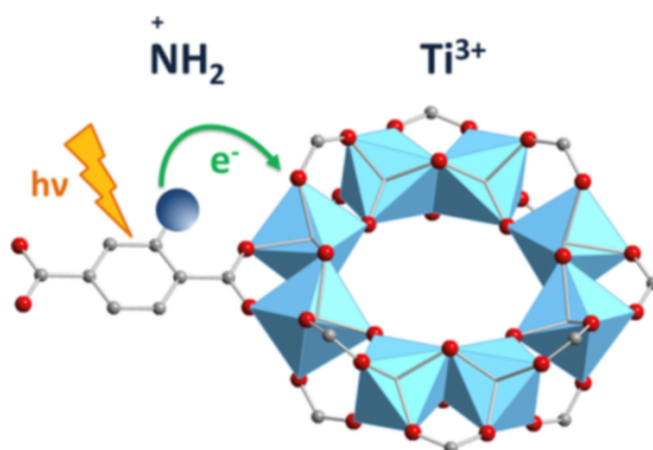
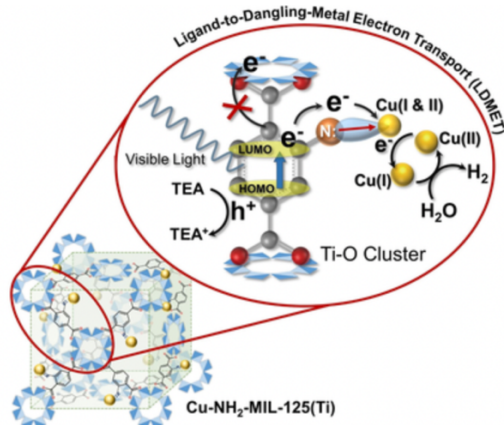
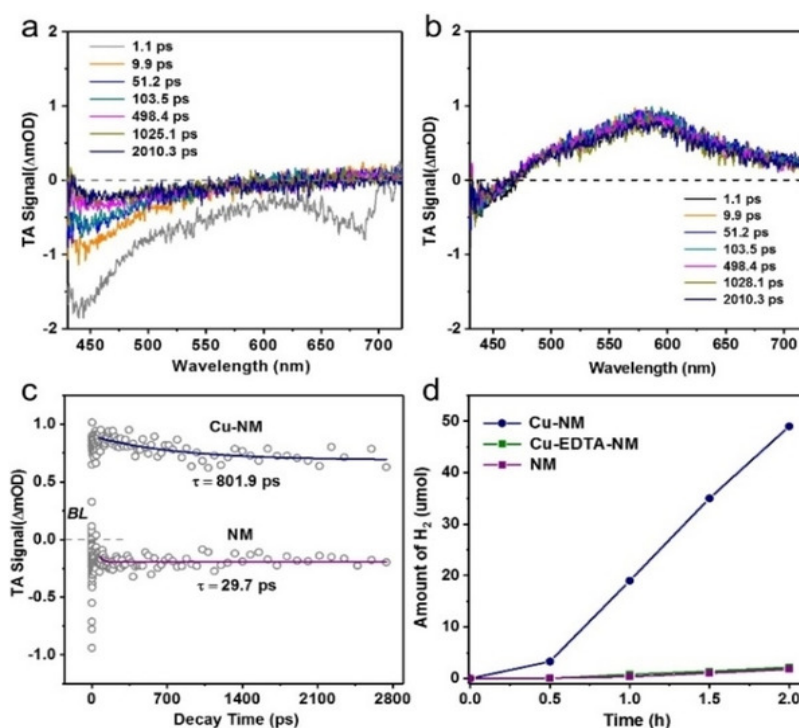


Figure 7 The ligand to metal charge transfer in MOFs<sup>23</sup>

Adding metal centre in MOFs is another strategy to improve charge separation. For example, in MIL-125-NH<sub>2</sub>, Cu is complexed with NH<sub>2</sub> to form the organic ligand. Figure 8 shows electron transfer paths from the organic ligand to Ti-O clusters and Cu centres in Cu-MIL-125-NH<sub>2</sub>(Ti). The real-time charge carrier dynamics is detected by Femtosecond TAS (fs TAS). In Figure 9 (a) and (b), fs TAS spectra show that Cu centre in MOFs is helpful for the charge separation as there are broad positive signals without obvious decay in presence of Cu. The lifetime of Cu-MOFs (801.9 ps) is 27 times longer than that of MOFs without Cu centre (29.7), which matches the photoactivity test.<sup>25</sup>

Figure 8 Electron transfer paths in Cu-MIL-125-NH<sub>2</sub>(Ti) <sup>25</sup>Figure 9 fs TAS spectra of MOF without Cu centre (a) and MOF with Cu centre (b); comparison of kinetics (c) and photocatalytic activity of MOF with/without Cu centre (d) <sup>25</sup>

The biggest difference of COFs from MOFs in structural component is that COFs are porous materials with only organic groups which are connected by covalent bonds. Similar to MOFs, precisely designed structures and targeted functions can be achieved in COFs by adjusting the organic linkages of COFs units, and 1D, 2D and 3D structures can be built. The physical and chemical properties of COFs can be changed, such as by the selection of building blocks, doping (metal/non-metal) and forming hybrid materials, which can enhance light absorption, charge transfer between hybrid materials and the

separation of electrons and holes<sup>26</sup>.

There are TAS studies of COF-based photocatalysts, and most of the lifetimes of photogenerated charges are from nanosecond to microsecond timescale, as shown in Figure 10, a bit longer than the lifetimes of MOFs which are usually less than several nanoseconds, but the lifetime of these COFs are still too short for photocatalytic reactions.

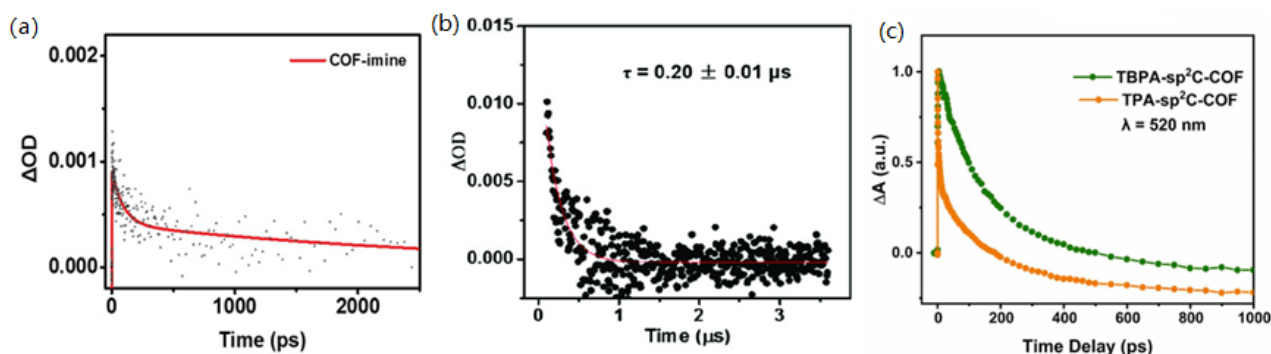


Figure 10 fs TAS kinetics of COF-imine<sup>27</sup> (a), COF: nTp-TTA/POM-1.1<sup>28</sup> (b), and  $sp^2C$ -COFs<sup>29</sup> (c)

Different strategies have been developed to enhance exciton dissociation efficiency of COFs, including incorporating donor-acceptor structures in COFs<sup>30</sup>, using co-catalyst<sup>31</sup>, building thin layer COFs<sup>32</sup>, and constructing COF-COF heterojunctions<sup>33</sup>.

There are three types of heterojunctions as shown in Figure 11<sup>34</sup>. Generally, Type II heterojunctions (with staggered bandgaps) are the commonly used structure for highly active organic photocatalysts such as  $g-C_3N_4$ <sup>35</sup>.

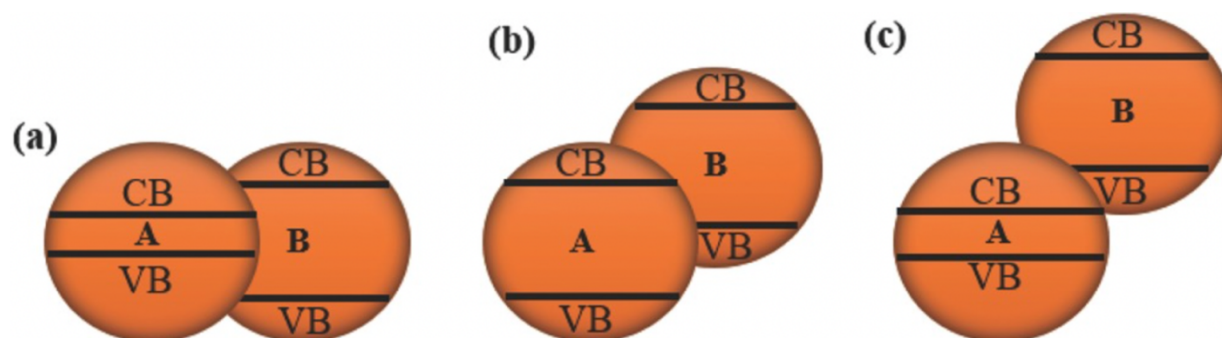


Figure 11 Three types of heterojunctions: type I (a), type II (b) and type III (c); A and B are semiconductors<sup>34</sup>

The schematic bandgap structure is shown in Figure 12. The conduction band of semiconductor B is higher than that of A. After light irradiation, the photogenerated electrons in B will transfer to the conduction band of A, and the photogenerated holes will transfer to the valence band of B. In the end, photogenerated electrons and holes are moving in opposite directions, which greatly helps the charge separation<sup>35</sup>. Therefore, building COFs and MOFs contain type II heterojunction could be a good strategy as well due to the ultrafast electron transfer, long-range charge delocalisation and long-term charge separation<sup>36,37</sup>.

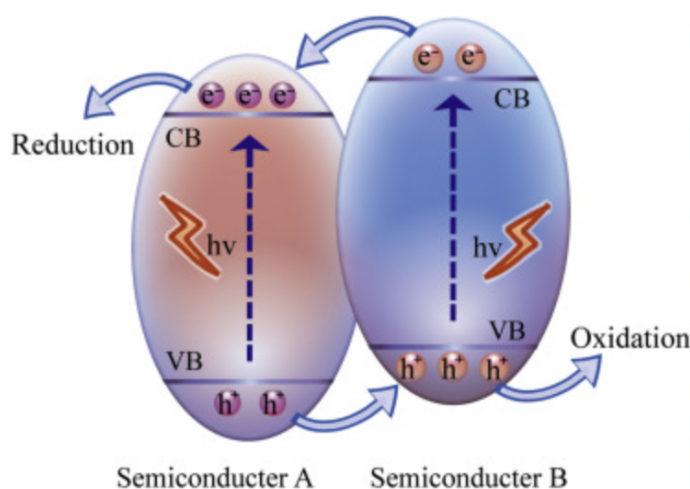


Figure 12 Optical band gap of type II heterojunction structure<sup>35</sup>

Surprisingly, recent reports about COFs heterojunctions still show very short lifetime for photocatalysis (from several nanoseconds to several microseconds) in dynamics study, and no comparison is made from photophysical perspective to identify if this heterojunction strategy is really helpful<sup>37-41</sup>. Herein, we want to understand the separation/migration mechanism of photogenerated carriers in these reticular photocatalysts, and hopefully this study could give a deeper insight in some of the current material design strategies.

## Chapter 2 Aims and Objectives

The aim of this project is to provide guidelines on the design of efficient reticular photocatalysts, by investigating the charge carrier dynamics in the selected reticular photocatalysts with some commonly applied strategies for efficiency improvement, such as adding co-catalysts, scavengers, or building heterojunctions.

For reticular photocatalysts, such as MOFs and COFs, there are many electron and hole transfer pathways due to the structural complexity, so it is difficult to understand the photocatalytic mechanism, especially when there are scavengers or co-catalysts in the system. By studying the transient absorption spectrum and decay kinetics of MOFs, we can indicate the potential of newly developed MOFs in photocatalysis. For example, there is barely photocatalytic data report of MIP-177-LT(Ti), a recent developed MOF which is very stable and easy for bulk preparation <sup>42</sup>.

The progress in investigation of MOFs synthesise and catalytic efficiency improvement has been considerable, however, the limited photophysical studies leads to a situation that there are very rare mechanistic instructions on how to build up these MOFs, and it is difficult to figure out the reason when some MOFs doesn't show good catalytic results.

After the end of the project, we hope to be able to understand the charge carrier behaviour in the selected MOFs and COFs, have an idea of the effectiveness of the heterojunction strategy, and provide further suggestions on the improvement these MOFs and COFs photocatalysts.

## Chapter 3 Method

### 3.1 Materials and Chemicals

Selected MOF samples are part of a European project METHASOL, which Durrant group is member. COF samples are within an ongoing collaboration between Durrant and McCulloch group.

Powder samples of MIL-125-NH<sub>2</sub>(Ti) and Cu loaded sample 2 wt% Cu@MIL-125-NH<sub>2</sub>(Ti) are from Prof. Nathalie Steunou, CNRS-ILV (Centre national de la recherche scientifique-Institut lavoisier de versailles, France). Powder samples of UiO-66-NH<sub>2</sub>(Zr), MIP-177-LT(Ti), 9wt%Cu@MIP-177-LT(Ti) and 12wt%Cu@MIP-177-LT(Ti) are from Dr. Georges Mouchaham, ENS-IMAP (Ecole normale superieure-Institute of porous materials, France).

The COFs samples including donor COF(D), acceptor COF(T), COF with donor-acceptor heterojunction structure (T), and 3 wt%Pt@COF with donor-acceptor heterojunction(T-Pt) are from Dr. Catherine Aitchison, McCulloch Group, University of Oxford. The samples were received as powder.

N,N-Dimethylformamide (DMF, solvent, purity>99.8%), Methanol (solvent, purity>99.8%) and L-Ascorbic acid (solid state) are from Sigma-Aldrich. Acetonitrile (ACN, high purity for HPLC) is from VWR. Water is from ultrapure water system.

### 3.2 Sample Preparation

#### 3.1 MOFs Samples

Solution samples were prepared both in solution and on film. Solution: 6.25mg/mL MOFs were dispersed in acetonitrile by sonicating the mixture for 1 minute, and then were put in cuvettes with light path-length of 1mm. Film samples were prepared by dropcasting, using 200 uL samples dispersion in ACN on top of glass with an area of 1cm×1cm and dry at room temperature.

#### 3.2 COFs Samples

First, 1.6 mg of COFs samples were dispersed in 3 mL of DMF (S<sub>1</sub>) by probe sonicating (Time: 2 min;

Pulser: 20 s on, 5 s off; Amplify: 30%. Run three times in total). Then, 0.4 mL  $S_1$  solutions was added into 1 mL water while sonicating ( $S_2$ ). The solutions  $S_2$  were diluted to the ideal concentrations for measurements in a mixture of DMF and Water (2:5 by volume).

### 3.3 Photophysical Study

#### 3.3.1 UV-Vis Absorption

All the MOFs film samples were measured by steady state UV-Vis absorption spectroscopy (Cary 7000, Agilent Technologies). A glass without sample was used as reference. All the COFs samples were measured in cuvettes (light path length: 2 mm) by Cary 60 UV-Vis spectroscopy, and a mixture solution of DMF and Water (2:5 by volume) in cuvette was used as reference.

#### 3.3.2 Photoluminescence (PL) Measurement

Both MOFs and COFs samples were measured in solution (acetonitrile as solution for MOFs samples and DMF + Water as solution for COFs) by Cary Eclipse Fluorescence Spectrophotometer.

#### 3.3.3 Transient Absorption Measurement

Transient absorption spectroscopy is a time-resolved pump-probe tool with laser as the excitation source. Sapphire laser system (Solstice) and Helios spectrometers (ultrafast systems) were used in ultrafast TAS. The excitation wavelength was tuned by optical parametric amplifier (TOPAS Prime) and frequency mixer (NirUVis). In ultrafast transient absorption spectroscopy system (fs-TAS, from femtosecond to nanosecond timescale), MIP-177(Ti) series of MOFs were excited at 320 nm (laser intensity: 750 nJ, without pin), UiO-66-NH<sub>2</sub>(Zr) was excited at 355 nm (laser intensity: 200 nJ, without pin), MIL-125-NH<sub>2</sub>(Ti) series of MOFs were excited at 400 nm (laser intensity: 300 nJ, without pin) and COFs series were excited at 400 nm (laser intensity: 70 nJ, without pin).

For transient absorption spectroscopies in microsecond to second timescale (slow TAS), the laser frequency was 9.4 Hz. The laser was generated by tunable laser systems (OPOTEK INC), and data were collected by Digital Phosphor Oscilloscope (Tektronix, DPO 3012) and X Series Multifunction

DAQ (National Instrument, NI USB-6361). The probe beam was from tungsten lamp (100 W, Bentham IL1) with monochromator (Photon Technology International, OBB-2001). A COF was excited at 355 nm, D and T COFs series were excited at 400 nm (laser intensity: 80 uJ, without pin).

MOFs samples were prepared on films and fully soaked in acetonitrile with continuous N<sub>2</sub> flow during measurements. COFs samples were in solution and degassed Ar before (20 minutes) the measurements.

### 3.3.4 Photoinduced Absorption Measurement

The set-up Photoinduced Absorption Spectroscopy (PIAS) is very similar to TAS (as shown in Figure 13<sup>43</sup>) except the pump light is a LED instead of a high intensity laser. The maximum wavelength of the LED used was 530 nm (from NewEnergy).

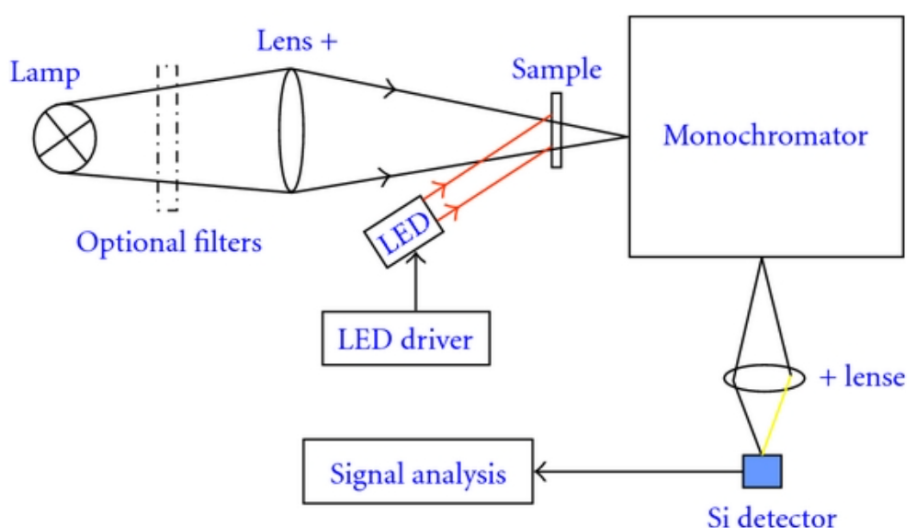


Figure 13 Schematic graph of PIAS setup<sup>43</sup>

## Chapter 4 Results and Discussion

### 4.1 Photophysical Study of MOFs

#### 4.1.1 MOFs Materials

Here we studied three series of MOFs and their composites for photocatalytic CO<sub>2</sub> conversion into methanol. They are Ti-based MOFs, MIL-125-NH<sub>2</sub>(Ti) and MIL-177-LT(Ti), and Zr-based MOFs, UiO-66(Zr)-NH<sub>2</sub>, as shown in Figure 14. MIL-125-NH<sub>2</sub>(Ti) is formed by cyclic octamers of TiO<sub>2</sub> octahedra with 1,4-benzenedicarboxylate (bdc), with the mono-aminated bdc-NH<sub>2</sub> as linkers<sup>44,45</sup>. It is proved that amino functionalised MIL-125(Ti) shows broader light absorption in visible light range and facilitates the photocatalytic reduction<sup>46</sup>. UiO-66-NH<sub>2</sub>(Zr) is Zr-based MOFs formed by terephthalate<sup>47</sup>. MIL-177-LT(Ti) (LT stands for low temperature form) is composed of a Ti<sub>12</sub>O<sub>15</sub> cluster secondary building unit with honeycomb crystal structure<sup>48</sup>. These materials are relatively stable with have good affinity for CO<sub>2</sub>, and they show better photocatalytic activity in materials screening. So we decided to explore the charge carriers dynamic in these materials.

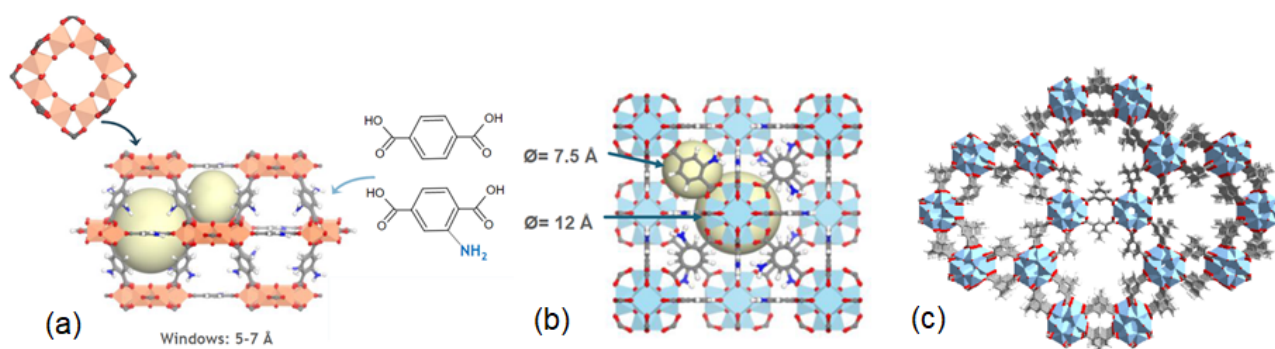


Figure 14 The Structure of (a) MIL-125-NH<sub>2</sub>(Ti)<sup>44</sup>, (b) UiO-66(Zr)/UiO-66(Zr)-NH<sub>2</sub><sup>47</sup> and (c) MIL-177-LT(Ti)<sup>48</sup>

#### 4.1.2 UV-Vis Absorption and Photoluminescence Study of MOFs Samples

We measured the UV-Vis absorption spectra of MIL-125-NH<sub>2</sub>(Ti) film and the composite of MIL-125-NH<sub>2</sub>(Ti) and Cu, with 2 wt% of Cu loading into the MOF channels (Figure 15). Samples showed an absorption feature at around 250-300 nm and 330-410 nm, which matches reported studies of this material<sup>49</sup>. Therefore, we chose to excite the MIL-125-NH<sub>2</sub>(Ti) sample at 400 nm on TAS studies (see below).

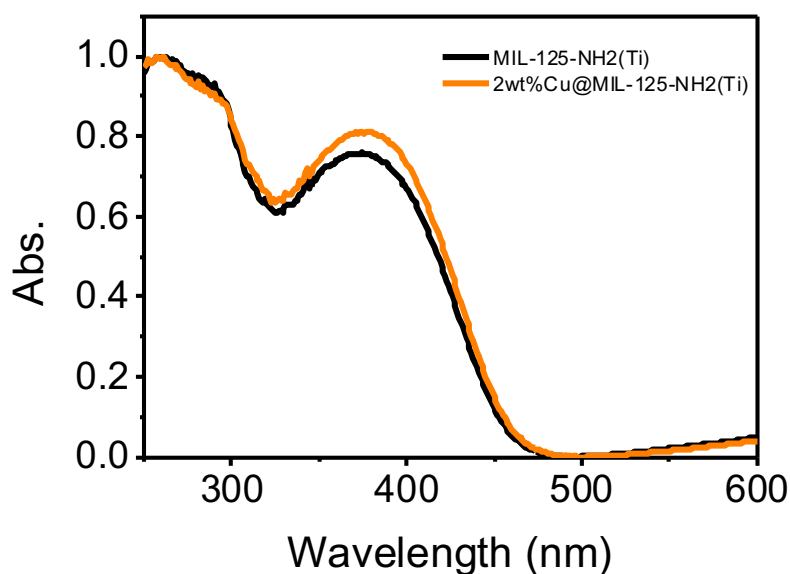


Figure 15 Normalised UV-Vis Absorption spectra of MIL-125-NH<sub>2</sub>(Ti) and 2 wt%Cu@MIL-125-NH<sub>2</sub>(Ti)

Then we turned to measure the photoluminescent (PL). Samples were prepared at the same UV-Vis absorption at the excitation wavelength. The PL spectra (Figure 16) shows that the loading of Cu nanoparticles had an effect of quenching the PL signal of pure MIL-125-NH<sub>2</sub>(Ti) (matches what the literature has reported)<sup>50</sup>, which may suggest that the Cu loading strategy may improve charge separation in MOFs.

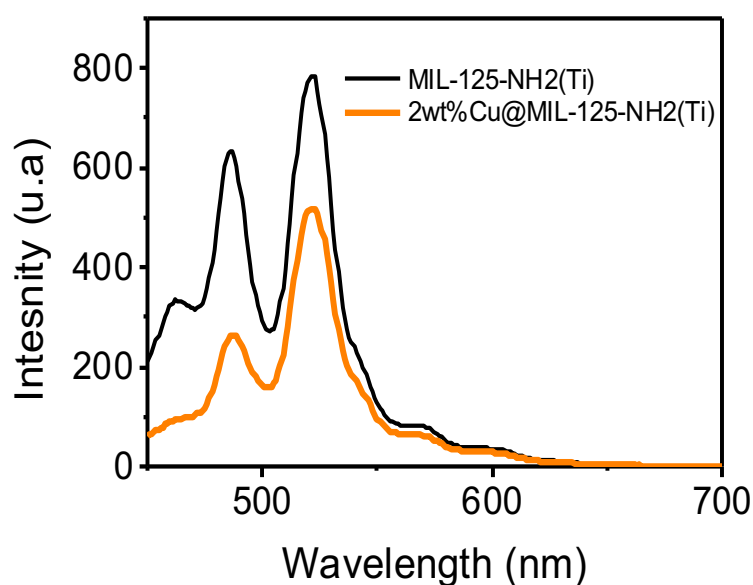


Figure 16 Photoluminescence spectra of MIL-125-NH<sub>2</sub>(Ti) and 2wt%Cu@MIL-125-NH<sub>2</sub>(Ti) in solution

For MIP-177-LT(Ti) series of MOFs, they show light absorption until around 350 nm (Figure 17). So we chose to excite the MOFs at 320 nm on TAS. Cu loading did not help improve the absorption, instead, the absorption decreased a bit, which may result from the lower portion of MIP-177-LT(Ti) (main light absorber) in the composite comparing the pure MOF.

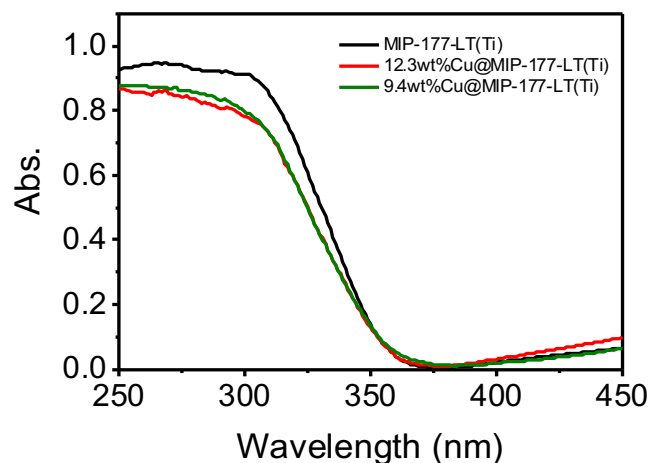


Figure 17 UV-Vis Absorption spectra of MIP-177-LT(Ti), 9.4wt% Cu@MIP-177-LT(Ti) and 12.3wt% Cu@MIP-177-LT(Ti)

Impressively, the PL signal of MIP-177-LT(Ti) was efficiently quenched after Cu loading, as shown in Figure 18. The PL quenching was more efficient than the observed in MIL-125-NH<sub>2</sub> above. This suggested the Cu loading strategy in MIP-177-LT(Ti) may improve charge separation more efficiently in this MOF. Further exploration on TAS is needed to prove this point.

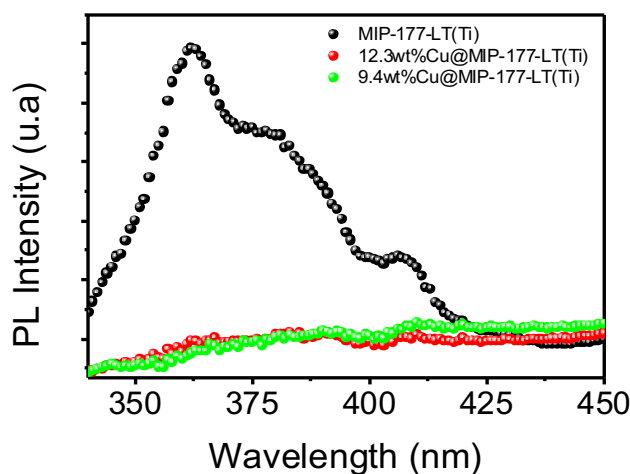


Figure 18 Comparison of photoluminescence spectra of MIP-177-LT(Ti), 9.4wt% Cu@MIP-177-LT(Ti) and 12.3wt% Cu@MIP-177-LT(Ti)

For UiO-66-NH<sub>2</sub>(Zr), the UV-Vis absorption spectrum shows the absorption range is around 210-270 nm and 340-410 nm (Figure 19) (there is also absorption at 300-400 nm in the literature<sup>51</sup>), and it has a PL signal from 435-530 nm (Figure 20) (same as reported data<sup>51</sup>). We chose to excite it at 350 nm on TAS.

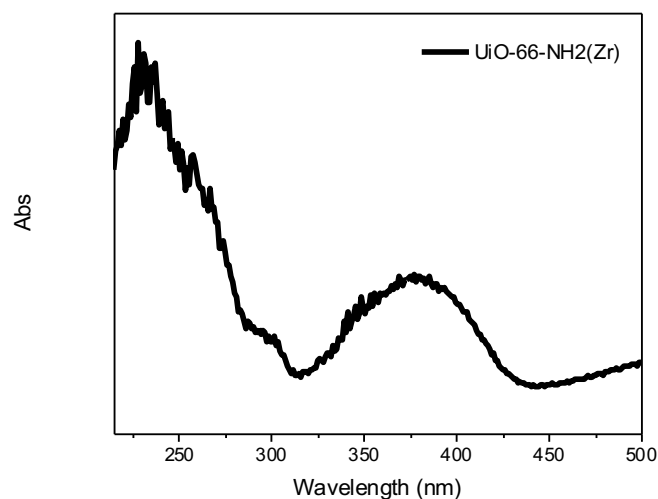


Figure 19 UV-Vis Absorption spectra of UiO-66-NH<sub>2</sub>(Zr)

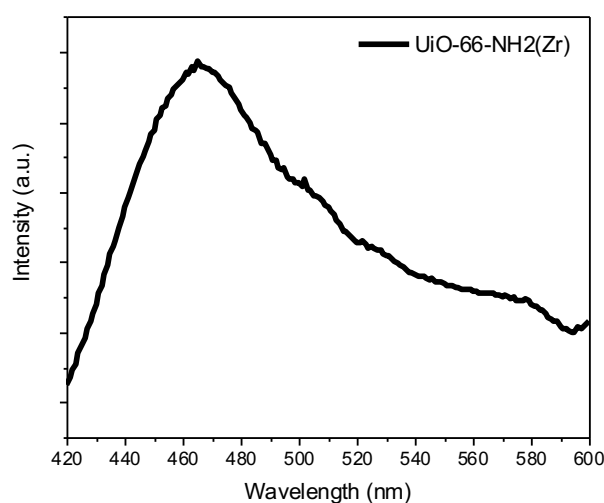


Figure 20 Photoluminescence spectra of UiO-66-NH<sub>2</sub>(Zr)

From the UV-Vis absorption measurement, a general shortcoming for these MOFs mentioned above (MIL-125-NH<sub>2</sub> series, MIP-177-LT series and UiO-66-NH<sub>2</sub>) is that they mostly absorb the light in ultraviolet range and have limited absorption for visible light, which isn't ideal for the fully utilization of sunlight, and it may be a factor limiting their photocatalytic efficiency.

### 4.1.3 Charge Carrier Dynamics Study of MOFs by Ultrafast Transient Absorption Spectroscopy

We turned to explore the charge carrier kinetics of the MOF by using ultrafast spectroscopies at the selected excitation wavelength based on our UV-Vis studies. First, the TA spectra of the single MOFs probed in the Visible range (400-800 nm) was explored. Then, TA of the composites was explored.

We excited the pure MIL-125-NH<sub>2</sub>(Ti), MIP-177-LT(Ti) and UiO-66-NH<sub>2</sub>(Zr) in ultrafast TAS system and get the spectra (Figure 21-23). They have broad transient absorption in the range of 500 nm-800 nm. UiO-66-NH<sub>2</sub>(Zr) and MIL-125-NH<sub>2</sub> decays very fast, while the main absorption of MIP-177-LT(Ti) in the spectrum doesn't change much with time, is still visible at 5.8 ns.

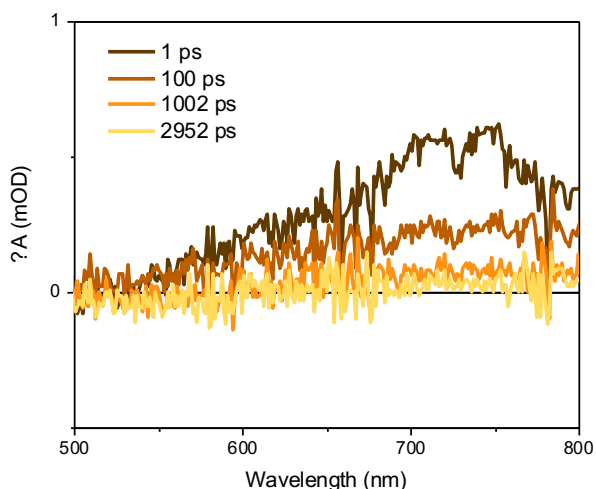


Figure 21 Ultrafast TAS spectra of MIL-125-NH<sub>2</sub>(Ti) (Excitation Wavelength: 400 nm, Laser Intensity: 300 nJ)

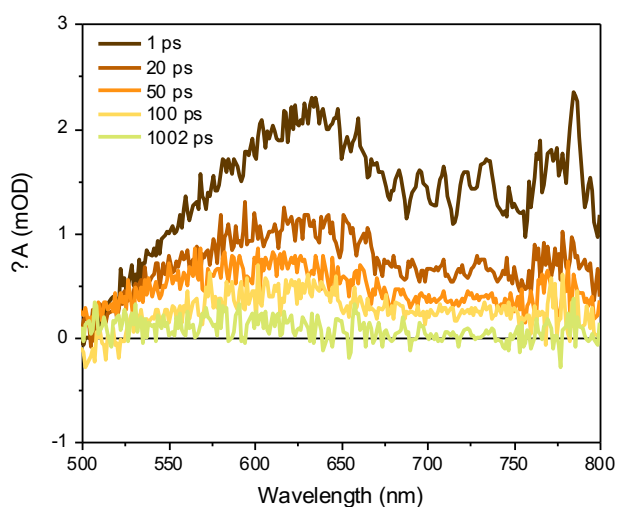


Figure 22 Ultrafast TAS spectra of UiO-66-NH<sub>2</sub>(Zr) (Excitation Wavelength: 350 nm, Laser Intensity: 200 nJ)

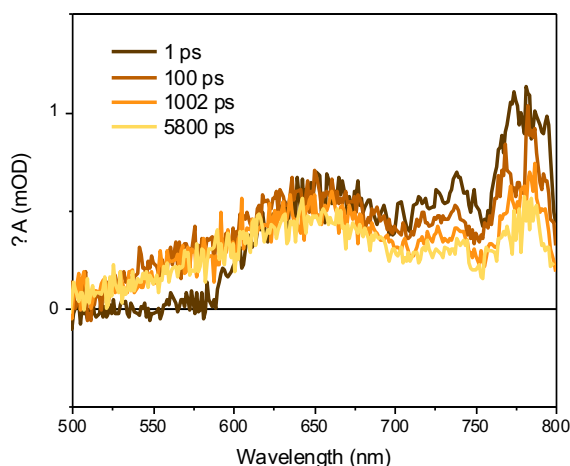


Figure 23 Ultrafast TAS spectra of MIP-177-LT (Ti) (Excitation Wavelength: 320 nm, Laser Intensity: 750 nJ)

The TA kinetics probed at 650 nm of these MOFs are shown in Figure 24. It is obvious that the signal of generated charges in MIL-125- $\text{NH}_2(\text{Ti})$  and UiO-66- $\text{NH}_2(\text{Zr})$  decay to zero within 1 ns, which is too fast to be helpful for photocatalysis. In contrast, MIP-177-LT(Ti) showed long-lived charges ( $>6$  ns). Even though the lifetime seems to be high for pure MOFs (usually from ps to ns)<sup>52</sup>, it is still considered as a fast decay for photocatalysis. Thus, strategies for improving charge separation are needed, such as structure functionalization, the built of composite, and the use of co-catalyst and sacrificial agent.

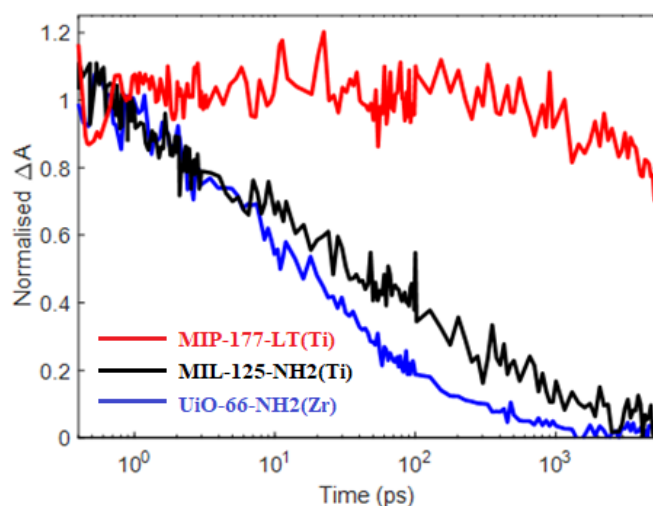


Figure 24 Kinetics Comparison of MIP-177-LT(Ti), MIL-125- $\text{NH}_2(\text{Ti})$  and UiO-66- $\text{NH}_2(\text{Zr})$

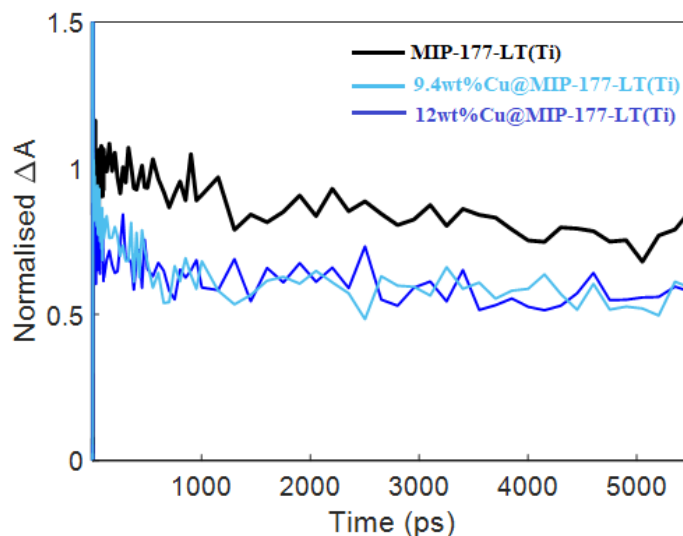


Figure 25 Kinetics Comparison of MIP-177-LT(Ti), 9.4wt%Cu@MIL-125-NH<sub>2</sub>(Ti) and 12.4wt%Cu@MIL-125-NH<sub>2</sub>(Ti)

As charges in MIP-177-LT(Ti) show longer lifetime than those in MIL-125-NH<sub>2</sub>(Ti), we studied the kinetics of MIP-177-LT(Ti), and the composite of MIP-177-LT(Ti) and Cu nanoparticles, with a Cu loading of 9.4 wt% and 12.3 wt%, respectively. In Figure 25, we can see that with Cu loading, the first part of the kinetics decays faster, which is indicative of electron transfer from MIP-177-LT(Ti) to Cu, in agreement with the PL quenching of MIP-177-LT(Ti) emission described above (Figure 18). This result indicates Cu co-catalyst loading might improve charge separation, so we would expect Cu@MIP-177-LT(Ti) composite materials to show better performance in photocatalysis than MIL-125-NH<sub>2</sub>(Ti). Besides, more studies are needed to understand the effect of adding hole scavengers.

However, for environmental and economic considerations, we want to design a photocatalytic system without adding external scavengers and co-catalysts, which is more challenging. Unfortunately, no photocatalytic CO<sub>2</sub> reduction activity is detected by MIL-125-NH<sub>2</sub>(Ti) or UiO-66-NH<sub>2</sub>(Zr) without co-catalysts and scavengers. Pure MIP-177-LT(Ti) shows higher activity but still have a space for improvement. These catalytic results can be explained by the kinetics study of these materials: the photogenerated charges are very short-lived, especially in MIL-125-NH<sub>2</sub>(Ti) and UiO-66-NH<sub>2</sub>(Zr). Therefore, it is significant to apply a more effective strategy to get longer-lived charges for photocatalysis, such as the preparation of heterojunctions.

## 4.2 Photophysical Study of COF Heterojunction

### 4.2.1 The Built of Donor-Acceptor COF Heterojunction

Building a heterojunction may be a potential strategy for better charge separation, as we usually expect the electron and holes separate more efficiently in the donor-acceptor interface. Herein, we got COF samples which are very similar to MOFs in structural, chemical and physical properties. And COFs with donor-acceptor heterojunctions are prepared to explore if the heterojunction strategy could be a breakthrough for improving the previous MOFs photocatalysts. Figure 26 shows the ligands and structure of donor (named as D) and acceptor (named as A).

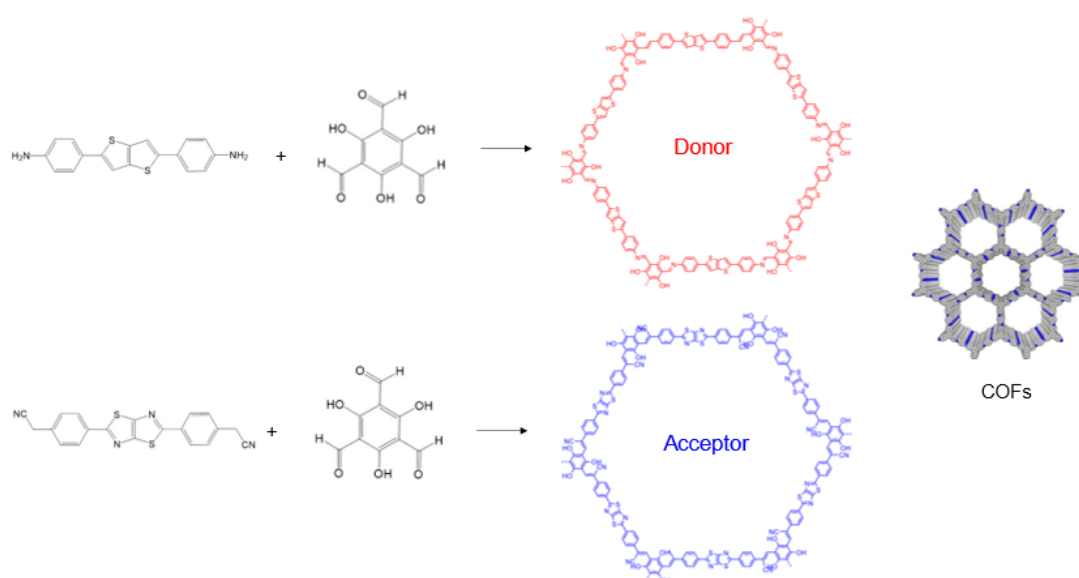


Figure 26 Donor and Acceptor Structure

And then, a layer-by-layer structure is built to form the COF heterojunctions (named as T)<sup>53</sup>, as shown in Figure 27, which is expected to behave better in charge separation.

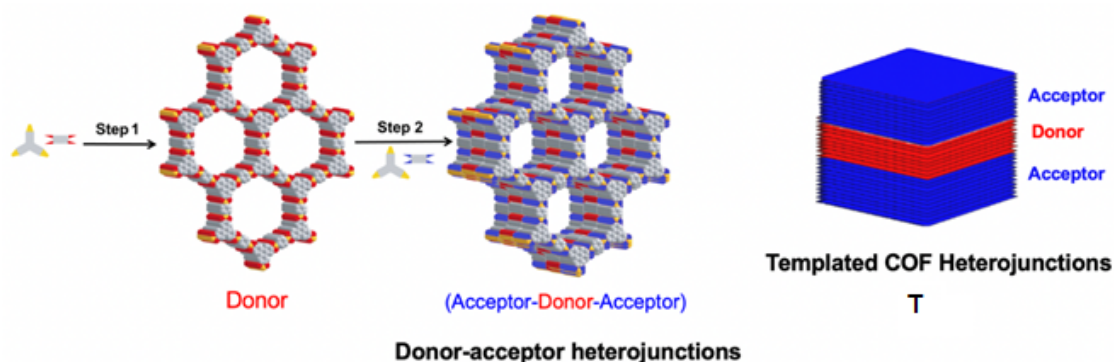


Figure 27 The built of Donor-Acceptor COF Heterojunction

#### 4.2.2 UV-Vis Absorption and Photoluminescence Study of COFs Samples

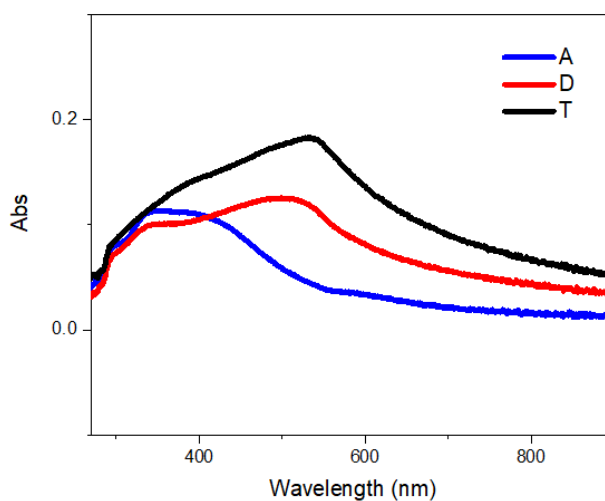


Figure 28 UV-Vis Absorption spectra of Donor (D), Acceptor(A) and COF Heterojunction(T) dispersed in DMF and water.

We prepare samples of A, D and T at the same concentration, and measure their UV-Vis absorption. As shown in Figure 28, the main absorption range of A is around 290-450 nm, and D and T show a broad absorption in UV-Vis range, with a peak at around 530 nm. Thus, we choose to excite them at 400 nm on ultrafast TAS. We can also see that the built of heterojunction improves the light absorption comparing D and A.

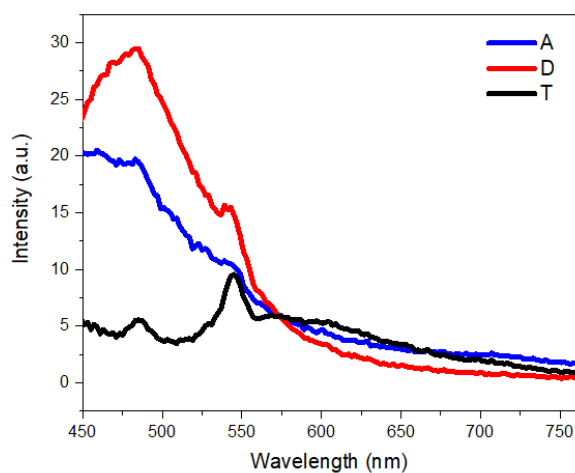


Figure 29 Photoluminescence spectra of Donor (D), Acceptor(A) and COF Heterojunction(T)

In photoluminescence measurement (Figure 29), even though the intensity of signals is very low, we can still see the PL quenching between 450-550 nm in T compared with the signal in A and D, which indicates improved charge separation in heterojunction.

### 4.2.3 Charge Carrier Dynamics Study of COF Heterojunction

#### 4.2.3.1 From Femtosecond to Microsecond Timescale

We explored the charge carrier dynamics behavior of A, D and T in fs-us timescale by ultrafast TAS. COFs were excited by laser with an excitation wavelength of 400 nm, and the ultrafast TA spectra are plotted with a time range from 1 ps to 4 ns in Figure 30-32. After the excitation of samples, first we observed a ground state bleaching (GSB), in agreement with their UV spectra (Figure 28) <sup>48</sup>. In addition, broad positive photo induced absorption signals were observed, with maximum amplitude at 625 nm, 665 nm and 725 nm for A, D and T respectively. The amplitude of the photogenerated transient species in T is higher than that in D or A, which indicates higher yield of photogenerated charges in the heterojunction.

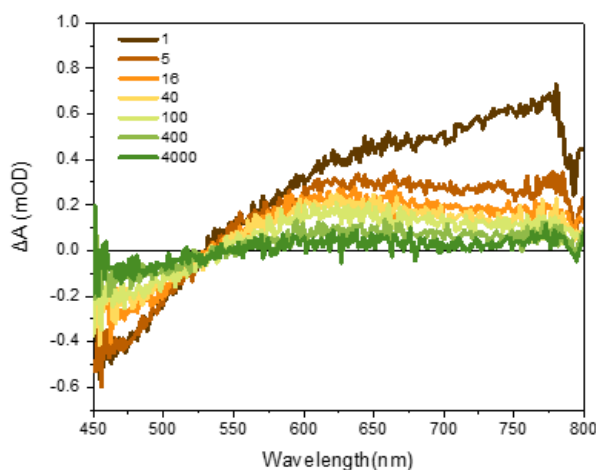


Figure 30 Ultrafast Transient Absorption Spectra of Acceptor (A) (Excitation Wavelength: 400 nm)

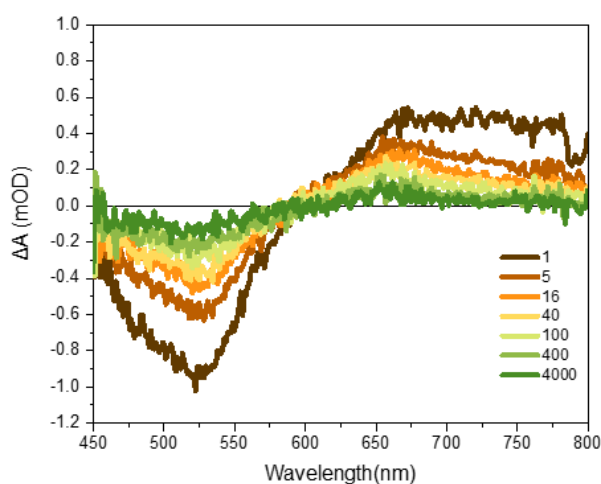


Figure 31 Ultrafast Transient Absorption Spectra of Donor (D) (Excitation Wavelength: 400 nm)

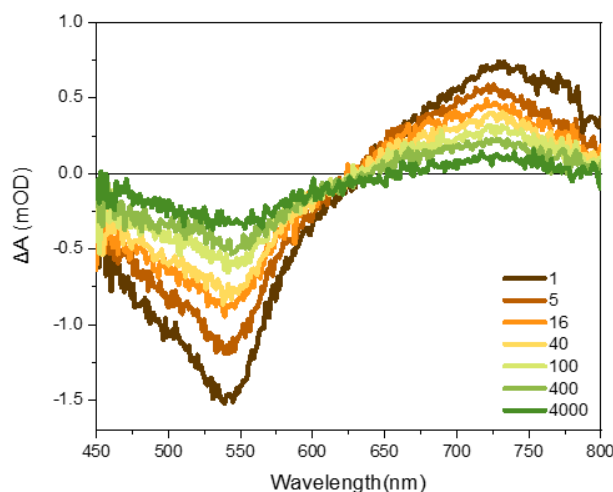


Figure 32 Ultrafast Transient Absorption Spectra of COF Heterojunction(T) (Excitation Wavelength: 400 nm)

As we can see in the ultrafast TA spectra, at a probe wavelength of around 526 nm, the transient absorption change ( $\Delta A$ ) is almost zero, which means there is almost no absorbance for A at this wavelength. At 526 nm, we compare the kinetics of D and T (Figure 33). In D, there are a few amount of photogenerated charges. And in T, there are more charges detected, which can be explained by the electron transfer from COF donor D to the acceptor COF A in the heterojunction, which helps charge separation in the donor-acceptor interface, so the charges in heterojunction are longer-lived.

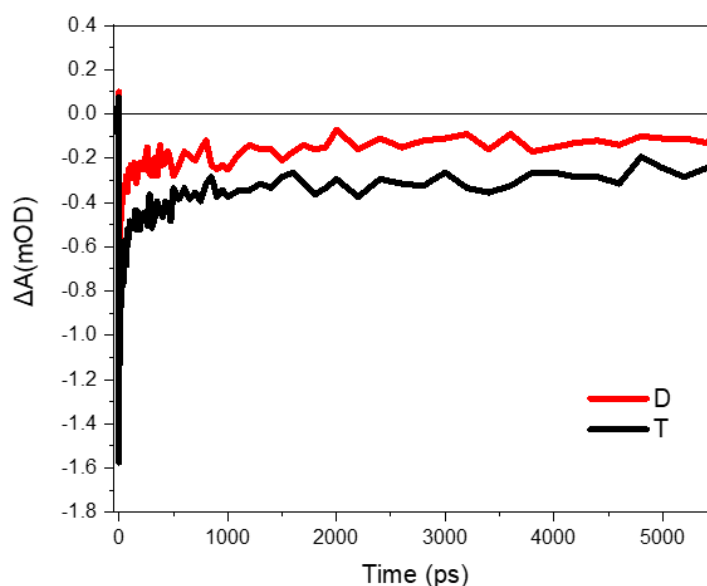


Figure 33 Kinetics Comparison of A, D and T (Probe 526 nm)

Then we analyzed the kinetics of T, A and D at a probe wavelength of 725 nm, where the absorption

change of species in heterojunction reaches a peak. We can see from Figure 34 that in heterojunction T there are much more longer-lived charges (>6 ns) than those in COFs A and D.

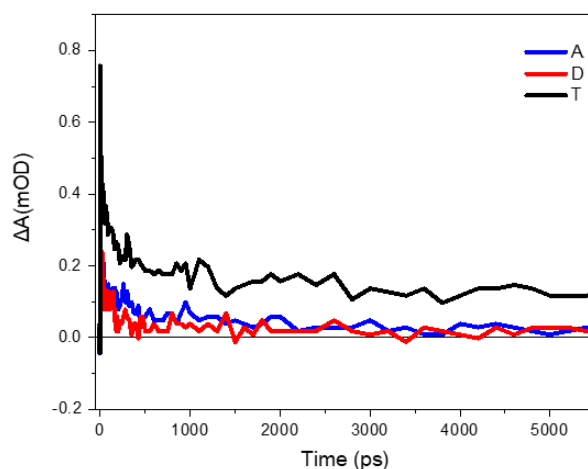


Figure 34 Kinetics Comparison of A, D and T (Probe 725 nm)

To identify what type of charge recombination happened in A, D and T in this timescale, we explored the kinetics at different excitation laser fluencies on ultrafast TAS. A faster TA kinetic decay with increasing fluency is indicative of bimolecular recombination of separated charges (electrons and holes); in contrast, fluence independent TA kinetics indicate monomolecular recombination (geminate recombination)<sup>54</sup>. Figure 35(left) shows the spectra of A (time: 1 ps) excited by laser with intensities from 50 nJ to 150 nJ. We can see the amplitude increases with the increase of laser intensity, which means there are more photogenerated species with higher laser intensity.

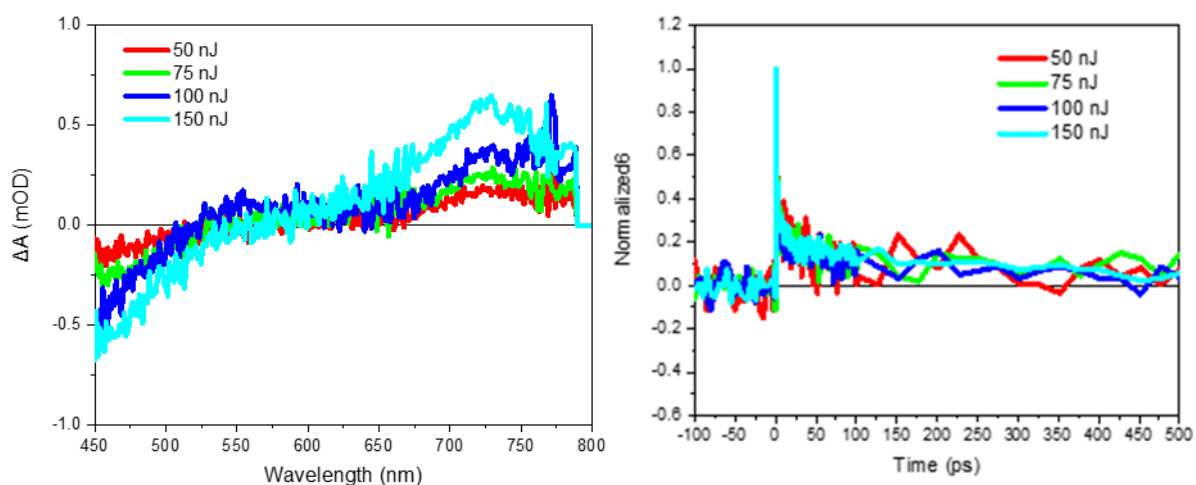


Figure 35 Ultrafast TAS Spectra (left) and Normalised Kinetics (right) of A Excited by Different Laser Intensities

At the probe wavelength of 725 nm, we normalize the kinetics of A with different laser intensities, as shown in Figure 35(right). The decay doesn't change with the increase of laser intensity and the lifetime of the photogenerated charges doesn't change as well, which indicates it is monomolecular recombination in this fs-us timescale, because even when there are more generated charges while laser intensity increase, the charge recombination rate remains the same, so it could only be geminate pair recombination<sup>54</sup>. If it were bimolecular recombination, with the increase of the laser intensity, the decay should be faster as there are more generated electrons and holes, so there will be higher possibility for them to recombine.

We observe the same trend on D and T (Figure 36, 37), which means in fs-us timescale, the charge recombination in A, D, and T is laser intensity independent, which is monomolecular recombination. We can conclude that there is not efficient charge separation in A and D in ultrafast timescale. And despite that there is higher yield of photogenerated charges in T, the photogenerated charges are not fully separate.

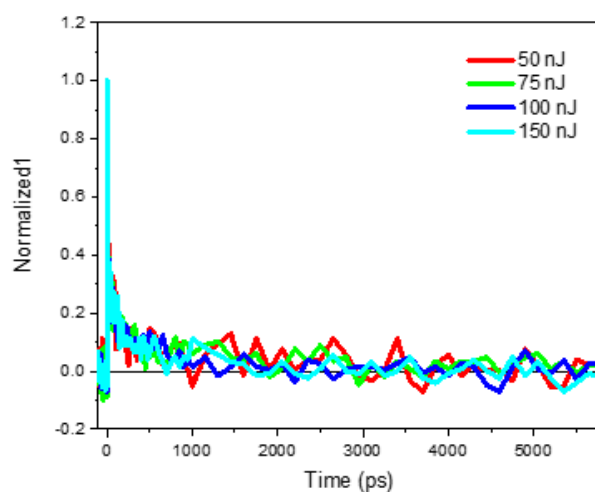


Figure 36 Normalized Kinetics of D by Different Laser Intensities on Ultrafast TAS

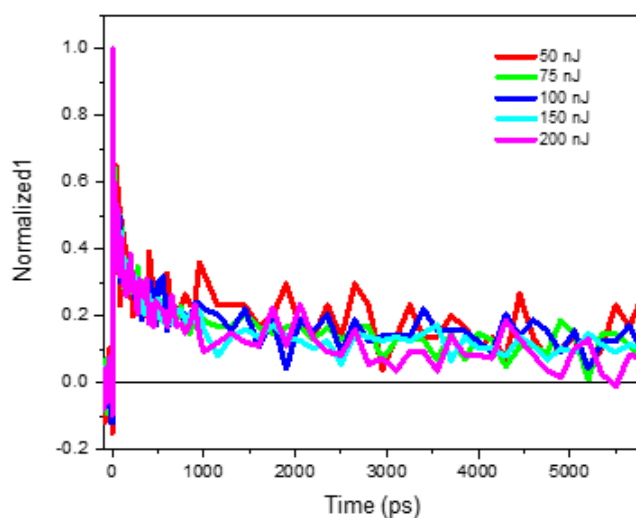


Figure 37 Normalized Kinetics of COF Heterojunction(T) with Different Laser Intensities on Ultrafast TAS

#### 4.2.3.2 From Microsecond to Millisecond Timescale (by Slow TAS)

Then we move on to a slower timescale, to explore the charge carrier behaviors in us-ms timescale. Figure 38-40 show the TAS spectra of A, D, T on Slow TAS ( $\mu\text{s}$ -ms timescale). The laser excitation wavelength: A-355 nm; D-430 nm; T-430 nm. The Tas spectra showed broad positive photoinduced absorption around 600-800 nm, which matches what we see on ultrafast TAS. It suggests the charges we observe on ultrafast TAS are long-lived enough to be detected in us-ms timescale.

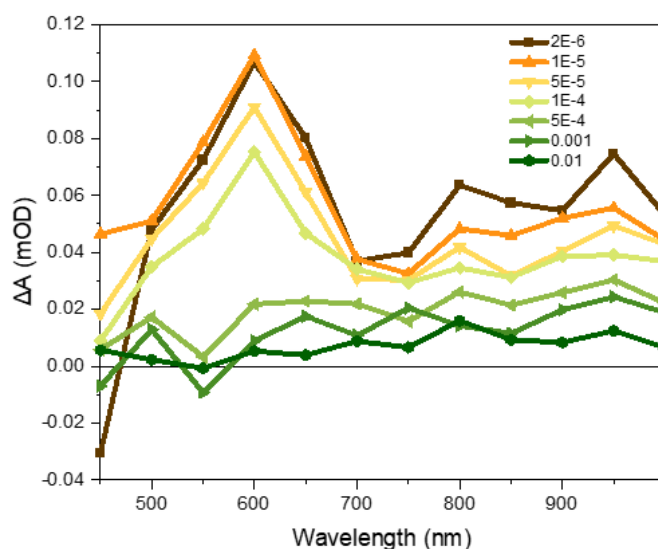


Figure 38 Transient Absorption Spectra of A on Slow TAS (Excitation Wavelength: 355 nm)

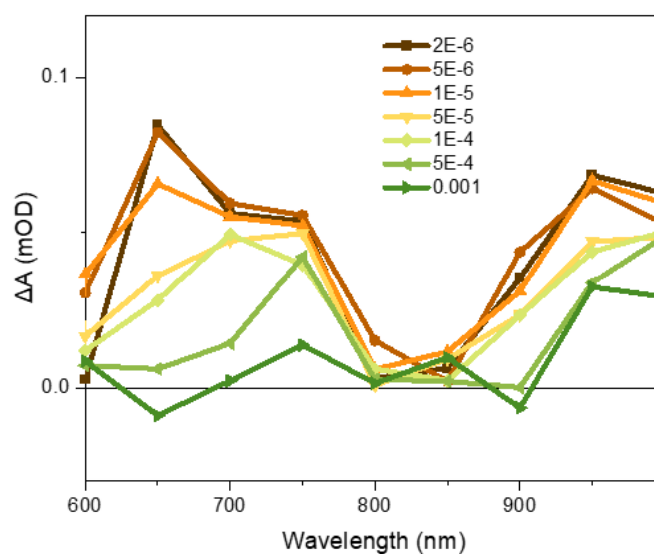


Figure 39 Transient Absorption Spectra of D on Slow TAS (plotted from 600 nm) (Excitation Wavelength: 430 nm)

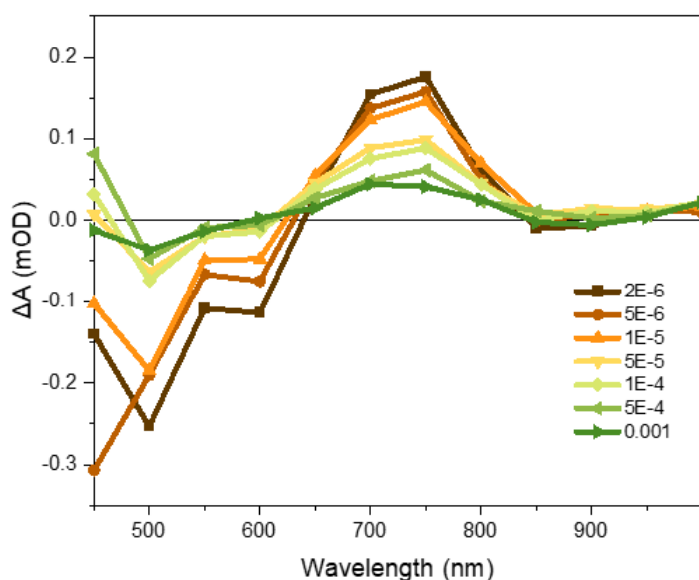


Figure 40 Transient Absorption Spectra of COF Heterojunction on Slow TAS (Excitation Wavelength: 430 nm)

We mainly focus on understanding the dynamics of photogenerated charges in the COF heterojunction T. In  $\mu\text{s}$ -ms timescale, we excite the heterojunction with different laser intensity from 50  $\mu\text{J}$  to 150  $\mu\text{J}$ , and compare the kinetics at the probe wavelength of 750 nm, where there are highest amount of photogenerated charges in the heterojunction, suggested by the TAS spectrum.

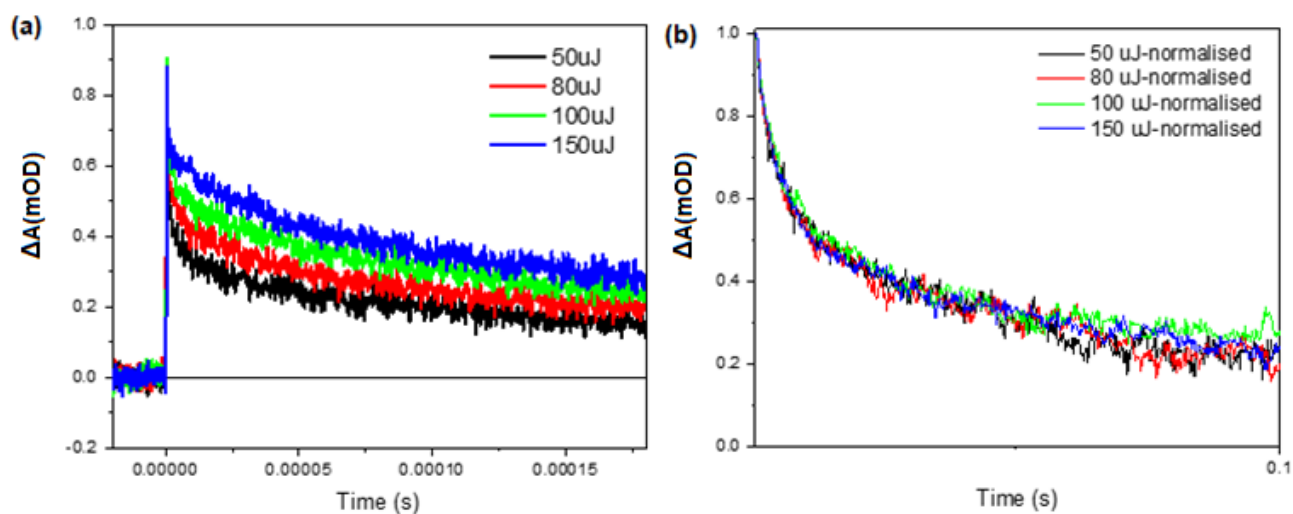


Figure 41 Kinetics of COF Heterojunction(T) Excited by Different Laser Intensities on Slow TAS

Figure 41(a) shows that with the increase of laser intensity, more charges are generated, but the decay and lifetime seem not to be affected. After normalizing the kinetics [Figure 41(b)], we can see the charges dynamics are laser independent in us-ms timescale. The change of laser intensity doesn't have an influence on the decay and lifetime of the photoexcited species. Therefore, the recombination of charges is monomolecular recombination as well in us-ms timescale.

#### 4.2.4 Charge Carrier Dynamics Study of COF Heterojunction with Co-catalyst and/or Scavenger

Furthermore, the composite of COF heterojunction and Pt nanoparticles is prepared for material optimization, co-catalyst used for proton reduction. At the same time, we also want to understand what kinds of transient species are generated in the COF heterojunction, so we use ascorbic acid as hole scavenger to study the kinetics change with/without the scavenger.

The pure COF heterojunction T, the composite of Pt nanoparticles (3wt%) and T (named as T-Pt), COF heterojunction with ascorbic acid added in system (named as T-AA), and the composite of T and Pt with ascorbic acid in system (named as T-Pt-AA) are studied on slow TAS. The excitation wavelength is 500 nm and their TAS spectra are shown in Figure 42-45.

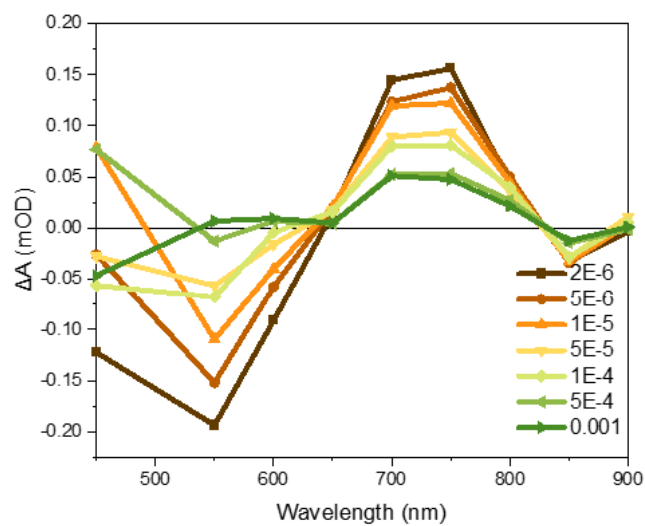


Figure 42 Transient Absorption Spectrum of T on Slow TAS (Excitation Wavelength :500 nm)

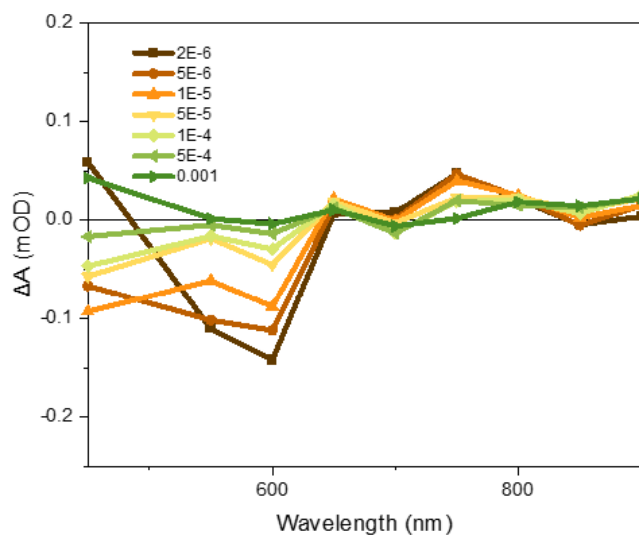


Figure 43 Transient Absorption Spectrum of T with 3wt% of Pt (T-Pt) on Slow TAS (Excitation Wavelength :500 nm)

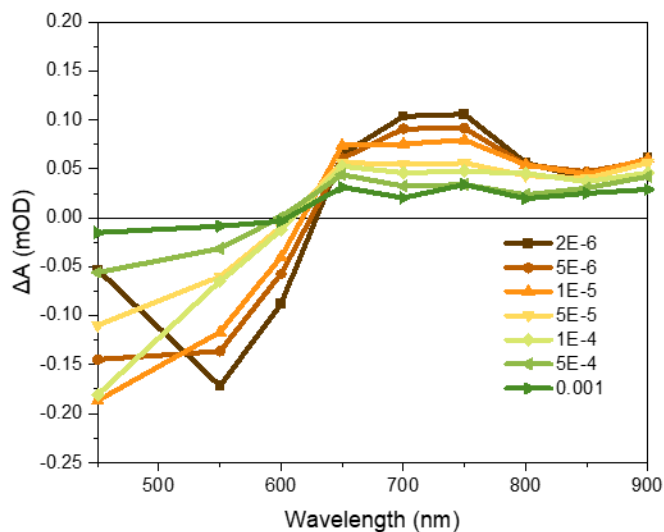


Figure 44 Transient Absorption Spectrum of T with Ascorbic Acid (T-AA) on Slow TAS (Excitation Wavelength :500 nm)

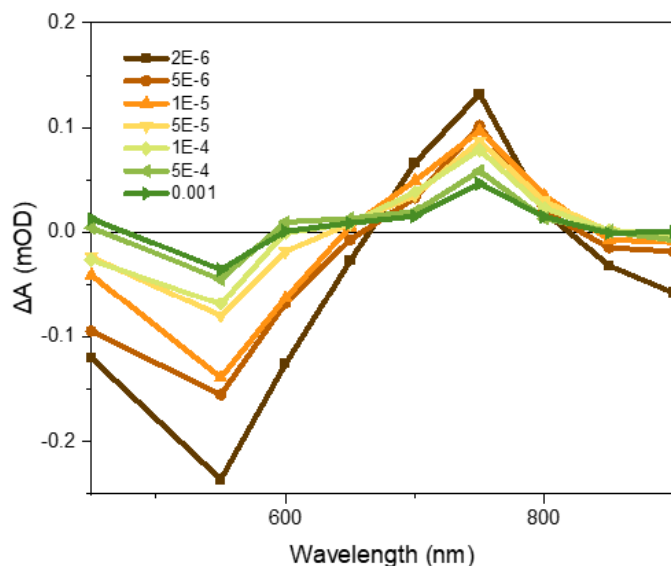


Figure 45 Transient Absorption Spectrum of T with 3wt% of Pt and Ascorbic Acid (T-Pt-AA) on Slow TAS (Excitation Wavelength :500 nm)

Still, we focus on the main positive signal from the photogenerated charges at around 650-800 nm in the spectra. The signal of the T-Pt composite (Figure 43) is lower than that of pure T heterojunction (Figure 42). With ascorbic acid in the solution (Figure 44), the signal is lower than that of T without ascorbic acid (Figure 42). While both Pt and ascorbic acid existing, the amplitude of the signal remains almost the same (Figure 45). This result may suggest that there are both holes and electrons contribute to this signal.

The kinetics at 750 nm shows that Pt as co-catalyst helps a little for a better charge separation. There may be electron transfer from COF heterojunction to Pt, but not very efficiently (Figure 46).

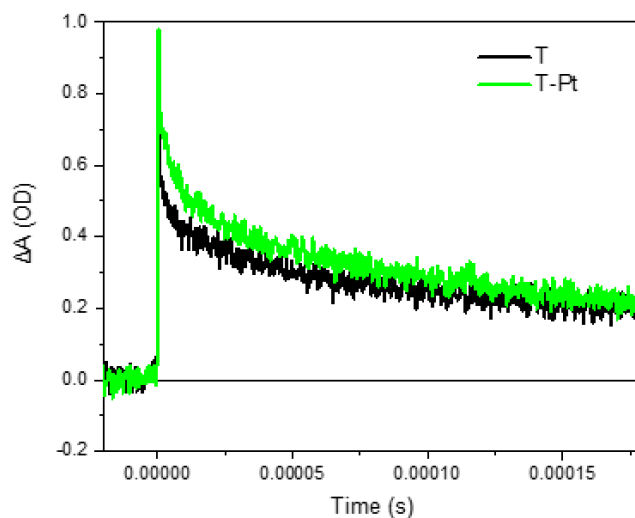


Figure 46 Kinetics Comparison of T and T with Co-catalyst Pt on Slow TAS

Meanwhile, ascorbic acid has an effect of quenching the signals. It is probably because the ascorbic acid takes holes away immediately which leads to an instant decrease of the signal of holes (Figure 47).

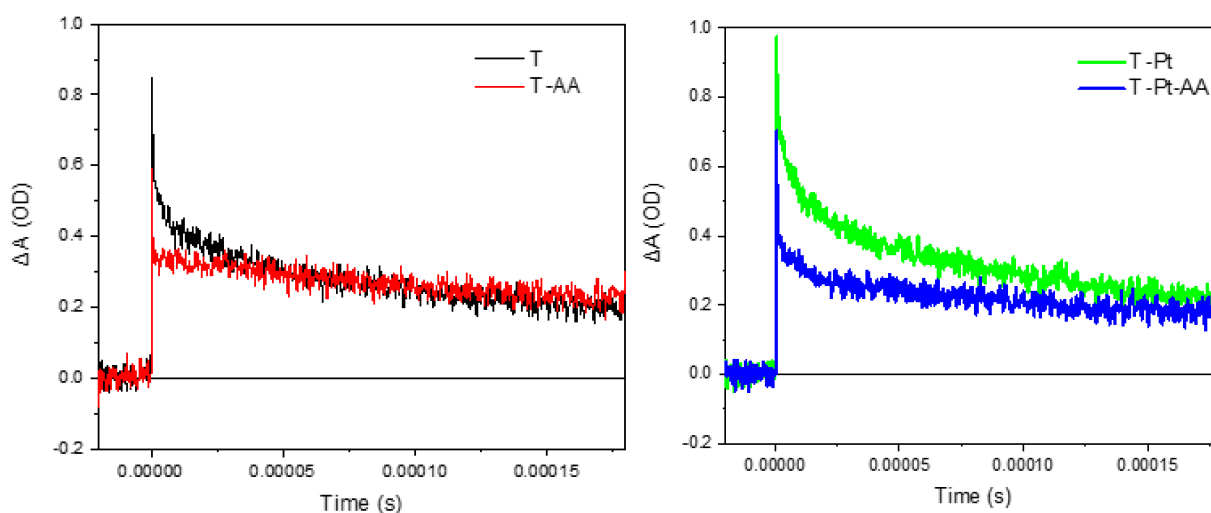


Figure 47 Kinetics Comparison of T (left) and T-Pt (right) with/without Ascorbic Acid on Slow TAS

However, there is no effect of Pt and ascorbic acid in exciton or charge separation in fs-us timescale, as shown in Figure 48. After normalizing the kinetics of T, T-AA, T-Pt and T-Pt-AA, all the kinetics completely overlap, so Pt and ascorbic acid don't affect decay and lifetime in this ultrafast timescale.

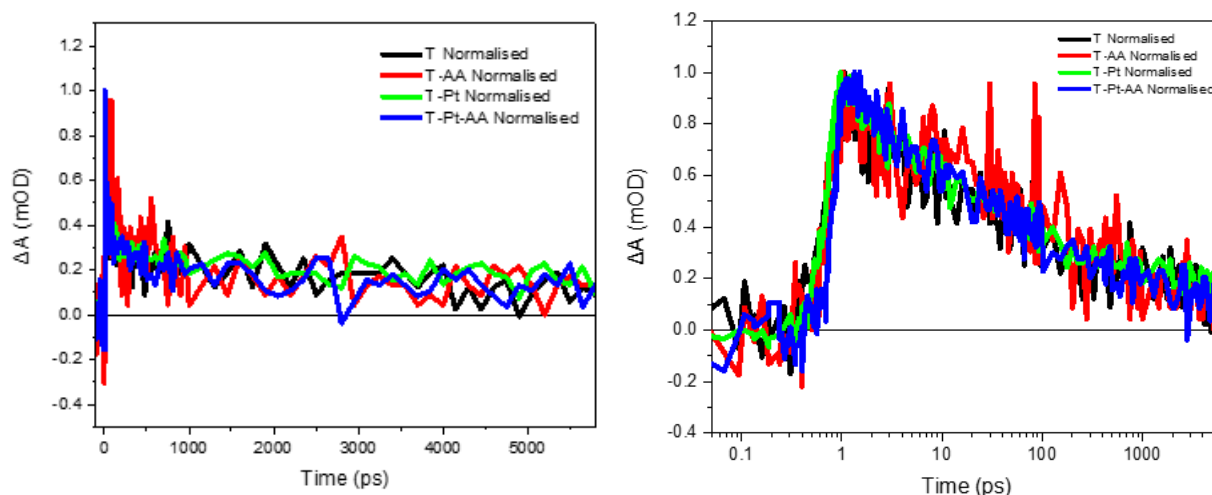


Figure 48 Charge Carrier Dynamics of T with Co-catalyst and/or Scavenger in fs-us Timescale

#### 4.2.5 Charge Carrier Dynamics Study of COFs by Photoinduced Absorption Spectroscopy

We turned to explore the kinetics on second timescale by using Photoinduced Absorption Spectroscopy. This is a technique used to track the photogenerated species under operando conditions, which means the measurement is under catalytic conditions<sup>55</sup>. We excite the COF heterojunction by LED light (10 w/cm<sup>2</sup>) with the excitation wavelength of 530 nm. The PIAS spectrum [Figure 49 (a)] of T is showed same absorption features than TA spectra described, with maximum at 700-800 nm as well.

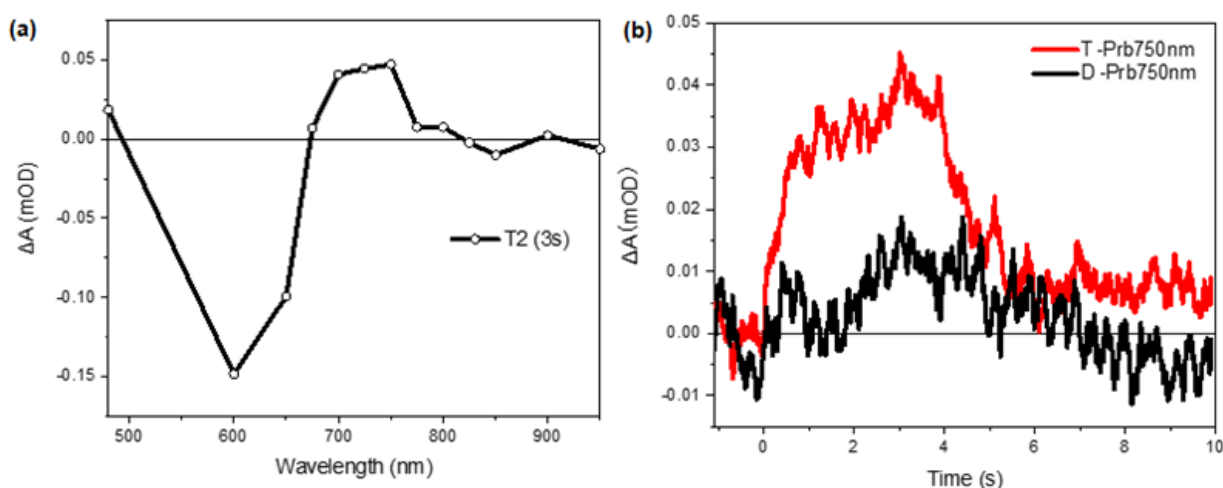


Figure 49 (a) PIAS Spectrum of T; (b) Kinetics Comparison of D and T on PIAS

Figure 49 (b) compares the kinetics of donor COF D and the COF heterojunction T at the probe wavelength of 750 nm on PIAS. When the LED light is on (4s), we observe a slow rise of the signal, which reach an equilibrium between charge generation and recombination at 4. This is indication of

equilibrium between formation and recombination of photogenerated charges. At 4 s, the light is off, and the charges decay. We can clearly see that the lifetime of charges in T is nearly 2 s, which is very long for COFs. At the same time, the lifetime of charges in D is much shorter, and it is much harder to generate charges by LED for D comparing T. There is no PIAS signal of A as it decays the fastest among these three COFs.

Kinetics of T, T-Pt, T-Pt-AA are compared on PIAS (Figure 50) (The negative signals indicate the settling of the samples). We can draw the same conclusion with that from TAS: the existence of Pt does help for charge separation, and while both Pt and ascorbic acid are in the system, it doesn't help with charge separation (there is no change with Pt-AA).

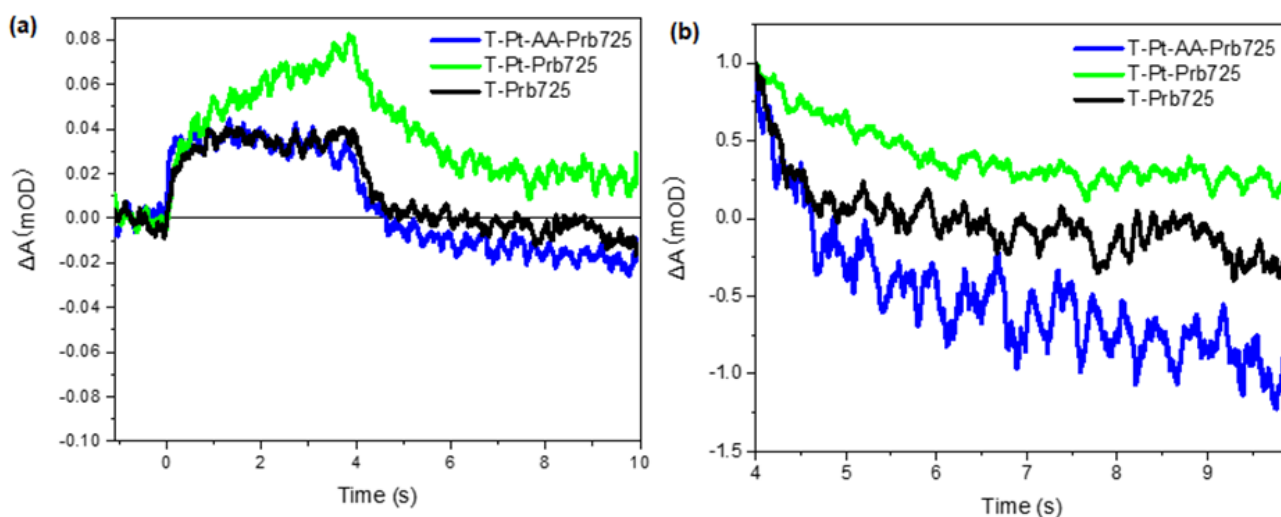


Figure 50 Kinetics Comparison of T, T-Pt and T-Pt-AA on PIAS (a) Normalized Kinetics at 4 s (b)

#### 4.2.6 Photocatalytic Activity

From the analysis above, we can indicate that the build of donor-acceptor heterojunction should be an effective strategy for improving the photocatalytic activity of COFs photocatalysts. As we expected, it is confirmed by the photocatalytic data of water splitting for hydrogen evolution. As shown in Figure 51, T shows significantly higher hydrogen production rate comparing D and A, and it also has much higher activity than the physical mixture of D and A, which means it is the heterojunction structure that helps with better charge separation. This result is very reasonable as we observe much longer-

lived charges in the COF heterojunction on TAS study, and it confirmed the validity of building heterojunction structure for improving the photocatalytic efficiency of COFs photocatalysts. However, these charges are not fully separate, as indicated in intensity dependence studies. This result suggests further optimization on the COF synthesis are needed to improve charge separation, including deeper study in crystallinity of the COFs.

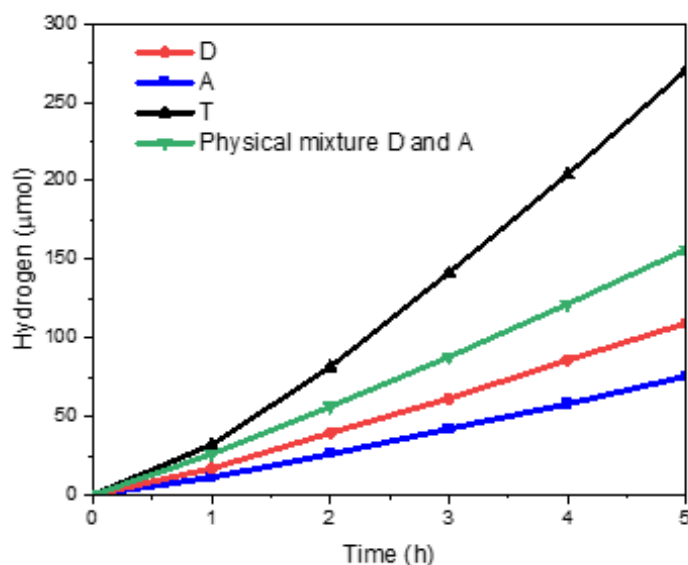


Figure 51 Photocatalytic Activity Comparison in Hydrogen Evolution (with 3 wt% Pt and ascorbic acid; data is measured by Dr. Catherine Aitchison, McCulloch Group, University of Oxford)

### 4.3 Comparison to a Broader Range of Photocatalysts

For COFs, except building the COF with donor-acceptor heterojunction or the COF-COF heterojunction we mentioned before, there is a study about COFs with cyano-substituted alkene linkages, which shows high efficiency of charge separation and charge transfer by fs-TAS. And the excited state absorption decay of COF-alkene (705 ps) is higher than those of COF-imine and COF-imide, but no exact lifetime is measured in slow TAS.<sup>56</sup> It provided a success example of functionalize the linkages of COFs with groups which have strong electron withdrawing and delocalization ability. Organic polymer photocatalysts, such as  $g\text{-C}_3\text{N}_4$  and conjugated polymers, are always discussed with COFs, as they are all polymeric semiconductors with similar structural features. It is proved by fs-TAS that the high crystallinity and reduced structural defects of carbon nitride are crucial for an efficient

charge carrier transfer<sup>57</sup>, which matches our suggestion about the COFs heterojunctions we studied in this project.

For MOFs, apart from the strategies we discussed above, substitute another kind of metal to the cluster is another effective way for improving charge separation. It is demonstrated there is higher photon-to-current efficiency in  $\text{NH}_2\text{-UiO-66(Zr/Ti)}$  than  $\text{NH}_2\text{-UiO-66(Zr)}$ , which comes from a slow recombination of photogenerated electrons and holes in  $\text{NH}_2\text{-UiO-66(Zr/Ti)}$  [lifetime > 200 us, which is so much longer than what we observed in  $\text{NH}_2\text{-UiO-66(Zr)}$  (lifetime = 1 ns)].<sup>58</sup> The charge dynamics study of  $\text{TiO}_2$  by TAS revealed the roles of crystal morphology and phase junction in photocatalysis.<sup>59,60</sup>, and it will be good to have a further TAS exploration and comparison of  $\text{TiO}_2$  (especially anatase) with the MOFs samples we have.

## Chapter 5 Conclusions and Future Work

### 5.1 Conclusions

In this research project, we studied the charge carrier behaviours of MOFs and COFs by transient absorption spectroscopy. For MOFs, we found that the loading of Cu into MIP-177-LT(Ti) channels may improve charge separation, and more studies about adding scavengers are needed. Besides, a more effective strategy to get longer-lived charges needs to be developed for efficient photocatalysis. For COFs, the charge carrier dynamics of a donor-acceptor COF heterojunction is studied by transient absorption spectroscopy from femtosecond to millisecond timescale. It is proved that the COF with heterojunction structure shows longer-lived charges than the donor COF and acceptor COF, and the heterojunction shows decay up to second timescale on photoinduced absorption spectroscopy, which is longer than most of reported single COFs. These results are consistent with the higher hydrogen evolution rate observed in the heterojunction COF relative to single COF.

Besides, our TAS studies in the heterojunction COF revealed slower, fluence-dependent, and decay kinetics, indicative of the monomolecular recombination of photogenerated charges, hindering the separation of the charges. The donor and acceptor COF also exhibits fluence-dependent and decay kinetics. The addition of Pt as cocatalyst and AA as hole scavenger, improve the charge extraction, in agreement with activity only observed in presence of this sacrificial scavenger; however, the charge extraction efficiency is very low.

The study of COF heterojunction explains why the add of scavengers and metal co-catalysts are not efficiently improving the photocatalytic activity in MOFs. And it is giving us an idea of building heterojunction structure in MOFs for a better charge separation so as to generate more and longer-lived charges for photocatalysis. The geminate recombination of electrons and holes in COF heterojunction also indicates the importance of improving crystallinity in reticular photocatalysts, for a further improvement of charge separation.

## 5.2 Future Work

Based on the analysis and conclusions above, we plan to follow up this idea of building heterojunction and study the heterostructure of MOFs and carbon nitride during my PhD here. It is already impressive for pure MIP-177-LT(Ti) to have a noticeable activity in photocatalytic H<sub>2</sub> evolution from formic acid with a quantum efficiency of 22%<sup>61</sup>. We are expecting a significant efficiency improvement of MIP-177-LT(Ti) in photocatalytic CO<sub>2</sub> reduction after the built of heterojunctions. Carbon nitride has good visible light absorption, high chemical and thermal stability, and very long-lived charges for photocatalysis<sup>62-64</sup>. Especially for PHI group, they can be good photocatalysts without co-catalysts. The transient absorption of selected pure carbon nitride will be studied and compared with pure MIP-177-LT(Ti). The portion of MIP-177-LT(Ti) and selected carbon nitride in the heterojunction will be determined by the amount of photoactive species produced in them, according to the kinetics. So eventually we will study the carrier dynamics in the heterojunction structure and have a deeper understanding of the formation, decay, recombination and transfer of photogenerated charge carriers in these photocatalytic systems.

## Acknowledgements

I want to express my gratitude to my supervisors, Prof. James Durrant and Dr. Soranyel Gonzalez-Carrero, for the numerous support they have given me on my project this academic year. I feel honoured and lucky to have them as my supervisors. The way they trained me makes me feel more confident about conducting my upcoming PhD projects independently. I am also grateful for Dr. Catherine Aitchison (University of Oxford) for sending me the COFs samples, so that I could have a chance to study and identify the behaviour of carrier dynamics in the heterojunctions, and prove from mechanism side that the built of heterojunction is a helpful strategy. And finally, I want to thank Prof. Nathalie Steunou (Institut Lavoisier de Versailles) and Dr. Georges Mouchaham (Centre National de la Recherche Scientifique -Institut Lavoisier de Versailles) for the MOFs samples, and all the other researchers from METHASOL project for inspiring communications.

## Acronyms

MOF: Metal-organic Frameworks

COF: Covalent Organic Frameworks

TAS: Transient Absorption Spectroscopy

PIAS: Photoinduced Absorption Spectroscopy

AA: Ascorbic Acid

A: The acceptor COFs

D: The donor COFs

T: The donor-acceptor heterojunction COFs

---

## References

- 1 H. L. Nguyen, *Advanced Energy Materials*, 2020, 10, 2002091.
- 2 A. Liu, M. Gao, X. Ren, F. Meng, Y. Yang, L. Gao, Q. Yang and T. Ma, *Journal of Materials Chemistry A*, 2020, 8, 3541–3562.
- 3 J. Xing, W. Q. Fang, H. J. Zhao and H. G. Yang, *Chemistry – An Asian Journal*, 2012, 7, 642–657.
- 4 Y.-Z. Chen, W.-H. Li, L. Li and L.-N. Wang, *Rare Metals*, 2018, 37, 1–12.
- 5 V. N. Gopalakrishnan, J. Becerra, E. F. Pena, M. Sakar, F. Béland and T. O. Do, *Green Chemistry*, 2021, 23, 8332–8360.
- 6 C. S. Diercks, Y. Liu, K. E. Cordova and O. M. Yaghi, *Nature Materials*, 2018, 17, 301–307.
- 7 A. Dhakshinamoorthy, A. M. Asiri and H. García, *Angewandte Chemie International Edition*, 2016, 55, 5414–5445.
- 8 Z. Wei, W. Wang, W. Li, X. Bai, J. Zhao, E. C. M. Tse, D. L. Phillips and Y. Zhu, *Angewandte Chemie International Edition*, 2021, 60, 8236–8242.
- 9 L. Xu, Y. Zhao, Z. Li, J. Wu, J. Cui, B. Tian, Y. Wu and Y. Tian, *ACS Applied Materials & Interfaces*, 2022, 14, 25278–25287.
- 10 R. Li, J. Hu, M. Deng, H. Wang, X. Wang, Y. Hu, H.-L. Jiang, J. Jiang, Q. Zhang, Y. Xie and Y. Xiong, *Advanced Materials*, 2014, 26, 4783–4788.
- 11 S. Corby, R. R. Rao, L. Steier and J. R. Durrant, *Nature Reviews Materials*, 2021, 6, 1136–1155.
- 12 R. Freund, O. Zaremba, G. Arnauts, R. Ameloot, G. Skorupskii, M. Dincă, A. Bavykina, J. Gascon, A. Ejsmont, J. Goscińska, M. Kalmutzki, U. Lächelt, E. Ploetz, C. S. Diercks and S. Wuttke, *Angewandte Chemie International Edition*, 2021, 60, 23975–24001.
- 13 D. Lenzen, J. Zhao, S.-J. Ernst, M. Wahiduzzaman, A. Ken Inge, D. Fröhlich, H. Xu, H.-J. Bart, C. Janiak, S. Henninger, G. Maurin, X. Zou and N. Stock, *Nature Communications*, 2019, 10, 3025.
- 14 S. Tao, L. Zhai, A. D. Dinga Wonanke, M. A. Addicoat, Q. Jiang and D. Jiang, *Nature Communications*, 2020, 11, 1981.
- 15 Y. Qian, F. Zhang and H. Pang, *Advanced Functional Materials*, 2021, 31, 2104231.
- 16 M. Zhang, Q. Shang, Y. Wan, Q. Cheng, G. Liao and Z. Pan, *Applied Catalysis B: Environmental*, 2019, 241, 149–158.

- 
- 17 H.-Q. Xu, S. Yang, X. Ma, J. Huang and H.-L. Jiang, *ACS Catalysis*, 2018, 8, 11615–11621.
  - 18 K. Sun, M. Liu, J. Pei, D. Li, C. Ding, K. Wu and H. L. Jiang, *Angewandte Chemie - International Edition*, 2020, 59, 22749–22755.
  - 19 S. Corby, R. R. Rao, L. Steier and J. R. Durrant, *Nature Reviews Materials*, 2021, 6, 1136–1155.
  - 20 C.-C. Wang, Y.-Q. Zhang, J. Li and P. Wang, *Journal of Molecular Structure*, 2015, 1083, 127–136.
  - 21 J.-D. Xiao, Q. Shang, Y. Xiong, Q. Zhang, Y. Luo, S.-H. Yu and H.-L. Jiang, *Angewandte Chemie International Edition*, 2016, 55, 9389–9393.
  - 22 J. G. Santaclara, F. Kapteijn, J. Gascon and M. A. van der Veen, *CrystEngComm*, 2017, 19, 4118–4125.
  - 23 J. G. Santaclara, M. A. Nasalevich, S. Castellanos, W. H. Evers, F. C. M. Spoor, K. Rock, L. D. A. Siebbeles, F. Kapteijn, F. Grozema, A. Houtepen, J. Gascon, J. Hunger and M. A. van der Veen, *ChemSusChem*, 2016, 9, 388–395.
  - 24 G. Wang, C.-T. He, R. Huang, J. Mao, D. Wang and Y. Li, *J Am Chem Soc*, 2020, 142, 19339–19345.
  - 25 X. Chen, S. Xiao, H. Wang, W. Wang, Y. Cai, G. Li, M. Qiao, J. Zhu, H. Li, D. Zhang and Y. Lu, *Angewandte Chemie International Edition*, 2020, 59, 17182–17186.
  - 26 H. Wang, H. Wang, Z. Wang, L. Tang, G. Zeng, P. Xu, M. Chen, T. Xiong, C. Zhou, X. Li, D. Huang, Y. Zhu, Z. Wang and J. Tang, *Chemical Society Reviews*, 2020, 49, 4135–4165.
  - 27 C. Mo, M. Yang, F. Sun, J. Jian, L. Zhong, Z. Fang, J. Feng and D. Yu, *Advanced Science*, 2020, 7, 1902988.
  - 28 H. Li, J. Liu, M. Wang, X. Ren, C. Li, Y. Ren and Q. Yang, *Solar RRL*, 2021, 5, 2000641.
  - 29 Y.-Z. Cheng, W. Ji, X. Wu, X. Ding, X.-F. Liu and B.-H. Han, *Applied Catalysis B: Environmental*, 2022, 306, 121110.
  - 30 S. Li, L. Li, Y. Li, L. Dai, C. Liu, Y. Liu, J. Li, J. Lv, P. Li and B. Wang, *ACS Catalysis*, 2020, 10, 8717–8726.
  - 31 T. Banerjee, F. Haase, G. Savasci, K. Gottschling, C. Ochsenfeld and B. v Lotsch, *J Am Chem Soc*, 2017, 139, 16228–16234.

- 32 R. Xiaomin, L. Chunzhi, K. Wanchao, L. He, T. Na, Y. Sheng, H. Linyan, W. Xiuli, L. Can and Y. Qihua, *CCS Chemistry*, 2021, 4, 2429–2439.
- 33 H. Dai, H. Li and Q. Yang, *Microporous and Mesoporous Materials*, 2022, 342, 112121.
- 34 F. Opoku, K. K. Govender, C. G. C. E. van Sittert and P. P. Govender, *Advanced Sustainable Systems*, 2017, 1, 1700006.
- 35 W. Sun, J. Zhu and Y. Zheng, *International Journal of Hydrogen Energy*, 2021, 46, 37242–37267.
- 36 Q. Yang, M. Luo, K. Liu, H. Cao and H. Yan, *Applied Catalysis B: Environmental*, 2020, 276, 119174.
- 37 S. Jin, X. Ding, X. Feng, M. Supur, K. Furukawa, S. Takahashi, M. Addicoat, M. E. El-Khouly, T. Nakamura, S. Irle, S. Fukuzumi, A. Nagai and D. Jiang, *Angewandte Chemie*, 2013, 125, 2071–2075.
- 38 S. Jin, M. Supur, M. Addicoat, K. Furukawa, L. Chen, T. Nakamura, S. Fukuzumi, S. Irle and D. Jiang, *J Am Chem Soc*, 2015, 137, 7817–7827.
- 39 W. Li, X. Huang, T. Zeng, Y. A. Liu, W. Hu, H. Yang, Y.-B. Zhang and K. Wen, *Angewandte Chemie International Edition*, 2021, 60, 1869–1874.
- 40 A. C. Jakowetz, T. F. Hinrichsen, L. Ascherl, T. Sick, M. Calik, F. Auras, D. D. Medina, R. H. Friend, A. Rao and T. Bein, *J Am Chem Soc*, 2019, 141, 11565–11571.
- 41 C. Xue, X. Fan, J. Zhang, D. Hu, X. L. Wang, X. Wang, R. Zhou, H. Lin, Y. Li, D. S. Li, X. Wei, D. Zheng, Y. Yang, K. Han and T. Wu, *Chemical Science*, 2020, 11, 4085–4096.
- 42 I. Bedja, *Advances in OptoElectronics*, 2011, 2011, 915123.
- 43 G. Capano, F. Ambrosio, S. Kampouri, K. C. Stylianou, A. Pasquarello and B. Smit, *The Journal of Physical Chemistry C*, 2020, 124, 4065–4072.
- 44 G. Capano, F. Ambrosio, S. Kampouri, K. C. Stylianou, A. Pasquarello and B. Smit, *The Journal of Physical Chemistry C*, 2020, 124, 4065–4072.
- 45 H. Wang, X. Yuan, Y. Wu, G. Zeng, X. Chen, L. Leng, Z. Wu, L. Jiang and H. Li, *Journal of Hazardous Materials*, 2015, 286, 187–194.
- 46 C. Gomes Silva, I. Luz, F. X. Llabrés i Xamena, A. Corma and H. García, *Chemistry – A European Journal*, 2010, 16, 11133–11138.
- 47 S. Wang, T. Kitao, N. Guillou, M. Wahiduzzaman, C. Martineau-Corcoc, F. Nouar, A. Tissot, L.

- Binet, N. Ramsahye, S. Devautour-Vinot, S. Kitagawa, S. Seki, Y. Tsutsui, V. Briois, N. Steunou, G. Maurin, T. Uemura and C. Serre, *Nature Communications*, 2018, 9, 1660.
- 48 M. A. Nasalevich, C. H. Hendon, J. G. Santaclara, K. Svane, B. van der Linden, S. L. Veber, M. v Fedin, A. J. Houtepen, M. A. van der Veen, F. Kapteijn, A. Walsh and J. Gascon, *Scientific Reports*, 2016, 6, 23676.
- 49 Z. Zhang, Y. Lin, J. Jin, L. Gong, Y. Peng, Y. Song, N. Shen, Z. Wang, K. Du and X. Huang, *Angewandte Chemie International Edition*, 2021, 60, 23373–23379.
- 50 M. Sachs, E. Pastor, A. Kafizas and J. R. Durrant, *The Journal of Physical Chemistry Letters*, 2016, 7, 3742–3746.
- 51 L. Francàs, C. A. Mesa, E. Pastor, F. le Formal and J. R. Durrant, *Rate Law Analysis of Water Splitting Photoelectrodes*, The Royal Society of Chemistry, 2018.
- 52 A. García-Baldoví, R. del Angel, G. Mouchaham, S. Liu, D. Fan, G. Maurin, S. Navalón, C. Serre and H. Garcia, *Active site imprinting on Ti oxocluster metal-organic framework for the photocatalytic hydrogen release from formic acid*, .
- 53 A. Savateev, D. Dontsova, B. Kurpil and M. Antonietti, *Journal of Catalysis*, 2017, 350, 203–211.
- 54 H. Schlomberg, J. Kröger, G. Savasci, M. W. Terban, S. Bette, I. Moudrakovski, V. Duppel, F. Podjaski, R. Siegel, J. Senker, R. E. Dinnebier, C. Ochsenfeld and B. v Lotsch, *Chemistry of Materials*, 2019, 31, 7478–7486.
- 55 J. Kröger, A. Jiménez-Solano, G. Savasci, P. Rovó, I. Moudrakovski, K. Küster, H. Schlomberg, H. A. Vignolo-González, V. Duppel, L. Grunenber, C. B. Dayan, M. Sitti, F. Podjaski, C. Ochsenfeld and B. v Lotsch, *Advanced Energy Materials*, 2021, 11, 2003016.